Visible-Light-Driven Newman-Kwart Rearrangement (NKR) by Nanomaterials

A thesis submitted to

Indian Institute of Science Education and Research Pune in partial fulfillment of the requirements for the BS-MS Dual Degree Programme

by

Mridul K. Vinod

(Reg No: 20201061)

Department of Chemistry

Indian Institute of Science Education and Research Pune

Dr. Homi Bhabha Road,

Pashan, Pune 411008, India.

April 2025

Under the guidance of

Prof. Pramod P. Pillai

All rights reserved

Certificate

This is to certify that this dissertation entitled **Visible-Light-Driven Newman-Kwart Rearrangement (NKR) by Nanomaterials** towards the partial fulfilment of the BS-MS dual degree programme at the Indian Institute of Science Education and Research, Pune represents study/work carried out by **Mridul K. Vinod** at the Indian Institute of Science Education and Research under the supervision of **Prof. Pramod P. Pillai**, Professor, Department of Chemistry, during the academic year **2024-2025**.

Signature of Student

Date: 27-03-25

Signature of Supervisor

This thesis is dedicated to

Amma, Acha & Minnu

(in my heart always)

Declaration

I hereby declare that the matter embodied in the report entitled '**Visible-Light-Driven Newman-Kwart Rearrangement (NKR) by Nanomaterials'** are the results of the work carried out by me at the Department of Chemistry, Indian Institute of Science Education & Research (IISER) Pune, under the supervision of Prof. Pramod P. Pillai and the same has not been submitted elsewhere for any other degree. Wherever others contribute, every effort is made to indicate this clearly, with due reference to the literature and acknowledgment of collaborative research and discussions.

Mridul K. Vinod

Reg No: 20201061

Acknowledgment

This thesis attained this shape with the help of many individuals. I want to thank all of them for their invaluable contributions.

I am deeply indebted to my supervisor, Prof. Pramod P. Pillai, for introducing me to research and for the opportunities, constant discussions, and helpful suggestions given to me. The insightful Monday group meetings and the opportunities to attend various conferences significantly shaped my understanding of science and how to maintain one's passion. I often had many health issues that hindered my lab work, and I want to give special mention to Sir for his patience, effort, and understanding in supporting me to shine through those challenges. I want to sincerely thank him for allowing me to be part of the *NanoAlchemy* family.

I am also extremely thankful to my TAC member, Prof. Angshuman Nag, for his valuable insights and discussions that significantly enhanced my understanding of the subject, especially during the early days, particularly around mid-year. Thank you for your guidance and for providing me with opportunities to learn from you.

I want to thank all the *NanoAlchemy* Lab members, both present and past, for their invaluable contributions. The present members — **Vanshika**, **Ankit**, **Shreya**, **Adhra**, **Shreya Prasad**, **Hisham**, **Rachit**, and **Asmita** — and the past members — **Sumit**, **Indra**, **Sriram**, **Aparna**, **Aiswarya**, **Namitha**, **Angela**, **Sandhra**, **Sruthy**, **Namitha K.S**, **Sujitha**, **Madhusmita**, and **Prakash** — have all played an essential role in creating an inspiring and encouraging environment that significantly enriched my learning experience.

My heartfelt gratitude goes to my direct mentors, **Radha Krishna Kashyap** and **Pradyut Roy**, who have been like brothers to me. They taught me the fundamentals of science and guided me in developing essential laboratory skills and adapting to the lab environment. Kashyap Bhaiyya, the man with the "golden touch," was always there when my project faced roadblocks, helping me find solutions with his remarkable skills and insights. Pradyut Bhaiyya taught me the value of discipline and how to communicate science effectively. I am incredibly fortunate to have had both of them as mentors.

I would also like to thank **Vanshika Di** for teaching me the importance of patience and perseverance, **Adhra Di** for showing me the value of kindness towards fellow lab members, **Ankit Bhaiyya** for demonstrating how to balance being fun and serious, and **Shreya Di** for inspiring me with her exceptional multitasking skills. Each of you uniquely shaped my journey, and I am genuinely grateful for the friendly and collaborative environment you created. The countless treats and "free chai" will always be fondly remembered and dearly missed.

I would also like to acknowledge IISER Pune for providing exceptional staff, faculty, students, facilities, and infrastructure that significantly contributed to my learning and research journey. I joined IISER Pune after getting totally hooked by a drone shot of the cricket ground in a YouTube video! The facilities had me awestruck, and here I am today!

I am grateful to all my friends who had been the greatest asset of my IISER life. I want to acknowledge — **Megha**, **Vijay**, **Ajma**, **Bhagya**, **Lakshmy**, **KS**, **Unni**, **Suresh**, **Bhageerath**, **DP**, **Akshay**, **Abhay**, **Akash**, **Prasad**, **Uday**, **Mehafus**, **LS**, **Utthara**, **Mufeeda**, **Anju, Shijil, Nandana**, **Muhsina**, **Avani** "**Gopalji**" and **Jewel** — for being with me in my ups and downs and being a constant source of comfort, reassurance, and a great listener. Special mention to **Aravind and Vijay** "Anna" for putting up with a messy roommate. Shout out to the **Vedikettu** team, where I could ace my football skills.

Lastly, I am eternally grateful to my family. Thanks, Amma and Acha. You have always motivated me to go beyond my comfort zone. Thank you to **Minnu** for your unwavering emotional support, **Muthoos** for the Saturday game nights that brought me joy, and my other relatives for their continuous love and encouragement.

As the saying goes, ***"The most beautiful view comes after the hardest climb."*** This journey has been challenging, but every struggle has shaped me into who I am today. Thank you to everyone who played a part in this climb. Thanks to Almighty!

Table of Contents

List of Figures

Abstract

The development of efficient and sustainable methods for energy-intensive organic transformations is crucial for advancing green chemistry. Sunlight could be a potential sustainable energy source for this purpose. Now, achieving chemical transformation with sunlight requires a fundamental understanding of the outcomes of light-matter interaction, particularly the roles of charge carriers and photothermal heat. Nanomaterials such as plasmonic nanoparticles (NPs) and quantum dots (QDs) have emerged as promising alternatives to molecular systems due to their enhanced light-harvesting capabilities and tunable properties. While extensive efforts have been made to improve the yields and selectivity of organic reactions in charge carriers and heat-driven processes independently, their combined influence within a single reaction framework remains largely unexplored. To address this, the current thesis investigates the use of plasmonic AuNPs as a thermoplasmonic heat source and core-only InP QDs as a photocatalyst for promoting the Newman-Kwart rearrangement (NKR): a thermally demanding transformation that converts O-aryl thiocarbamates into S-aryl thiocarbamates. The NKR was chosen both for its synthetic significance in thiol preparation from phenols and for its ability to exhibit distinct mechanistic behavior when driven by either charge carriers or heat. Under optimized conditions, yields of ~54% with InP QDs and ~23% with AuNPs were achieved utilizing charge carriers and photothermal outcomes, respectively. Although these yields are modest compared to conventional methods, this study introduces a unique dual activation strategy that expands the scope of light-driven NKR reactions. Future improvements in catalyst design and reaction conditions may enhance efficiency and selectivity, making this a valuable step toward sustainable organic synthesis.

Chapter 1: Introduction

The increasing demand for sustainable chemical production has driven significant research toward energy-efficient and environmentally friendly methods. Solar energy has emerged as a promising alternative due to its abundance, renewability, and potential to drive chemical transformations.[1-2] Harnessing solar energy effectively relies on understanding light-matter interaction, a fundamental process that facilitates the conversion of light energy into useful chemical outcomes. By exploring this interaction, researchers have developed innovative strategies to achieve efficient and sustainable synthesis pathways.[3]

The choice of material plays a crucial role in optimizing light-matter interaction for chemical transformations. Materials with strong light absorption properties are essential for harnessing solar energy effectively. Various classes of materials have been extensively studied for this purpose, including molecular systems, bulk semiconductors (SCs), quantum dots (QDs), and plasmonic nanoparticles (NPs). These materials offer distinct advantages based on properties such as charge carrier lifetime, mobility, and light absorption range. (**Figure 1a**) QDs and NPs have emerged as powerful candidates due to their unique and size-tunable optoelectronic properties.[4-17] These nanomaterials offer significant advantages in driving light-matter interactions, and their roles in both charge carrier generation[18-21] and heat generation[22-25] have been extensively studied over the years.

Quantum dots (QDs) stand out because of their size-dependent electronic properties, allowing for precise bandgap tuning. This tunability enables QDs to absorb light across a broad range of wavelengths, generating electron-hole pairs essential for driving photocatalytic reactions. The high stability and long carrier lifetime of QDs further enhances their ability to sustain reactions under prolonged light exposure. These characteristics make QDs ideal for activating reactions that require the efficient generation of charge carriers, such as in photocatalysis. In contrast, plasmonic nanoparticles (NPs) offer another advantage in light-driven reactions: the ability to generate localized heat upon light absorption. When irradiated with light, plasmonic NPs undergo plasmonic resonance, converting light energy into heat. This highly

concentrated localized heating can activate reactions that require thermal energy, such as those driven by thermoplasmonic effects. The precise control over heat generation provided by NPs is crucial for driving reactions that depend on thermal activation, and it is this capability that makes them valuable for a wide range of reactions that require heat as an energy source. [22-25]

a)

Type of material	Extinction coefficient ($M^{-1}cm^{-1}$)	Carrier concentration (cm^{-3})	Lifetime of charge carriers	Diffusion length/Mobility
Molecular systems	10^3-10^5	low	A few ns	-
Bulk semiconductors	10^4-10^6	10^{12}-10^{16}	ps to few ns	10-few 100's nm/ 10-1500 $cm^2V^{-1}s^{-1}$
Quantum dots	10^4-10^6	10^{18}-10^{20}	A few ns to 200 ns	10-100 nm/ 50-5000 $cm^2V^{-1}s^{-1}$
Plasmonic metals	10^8-10^{10}	10^{23}	1-100 fs	5-50 nm

b)

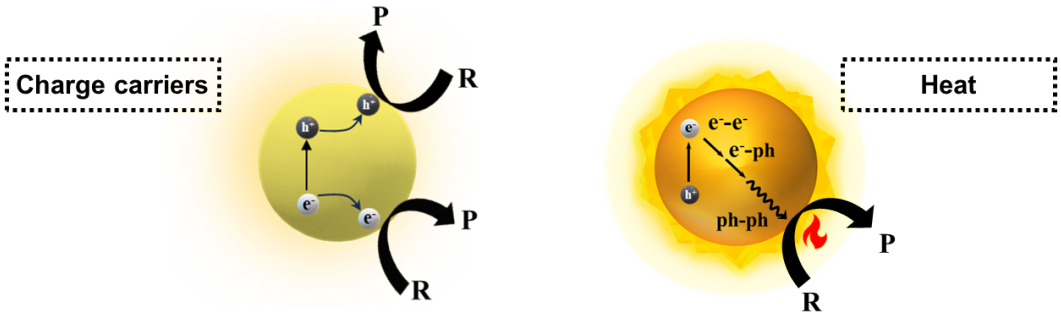

Figure 1: a) Classification of materials based on light-absorption properties. b) Representative diagram of light-matter interaction in nanomaterials; QDs (left) and NPs. (right)

While the individual roles of QDs and NPs in facilitating organic transformations are well-established, their combined potential to generate charge carriers and localized heat within a single system remains underexplored. This presents an opportunity to investigate a dual activation strategy that leverages both properties, potentially improving reaction efficiency and selectivity. To address this, the current thesis aims to evaluate the effectiveness of nanomaterials in driving an energy-intensive organic transformation: the Newman-Kwart rearrangement (NKR). By integrating charge carrier generation and photothermal effects within a unified system, our approach seeks to demonstrate a more versatile and unconventional method for NKR reaction.

The Newman-Kwart rearrangement (NKR) is a well-known thermal rearrangement widely employed for synthesizing S-aryl thiocarbamates from their corresponding O-

aryl thiocarbamates.[26-27] Before the reports by Kwart and Evans in 1966, followed by Newman and Karnes later that same year, no widely applicable and efficient method existed for converting phenols into thiophenols. Hence, this transformation holds significant value in organic synthesis due to its role in producing aryl thiols, which are key building blocks in pharmaceuticals, agrochemicals, and materials science.[28-31] The NKR's ability to selectively introduce sulfur-based functional groups makes it indispensable in constructing complex molecular frameworks.

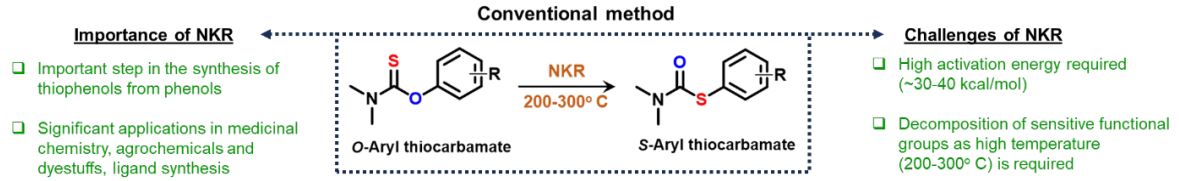

Figure 2: Summary of importance and challenges in Newman-Kwart rearrangement (NKR).

While the NKR is an effective method, several limitations often hinder its practical application. Conventional NKR reactions require prolonged heating at high temperatures (typically 200–300°C, depending upon the substrate of choice) to induce the desired rearrangement.[26-27]These extreme conditions consume significant energy and increase the risk of substrate decomposition and reduced yields, particularly for molecules containing thermally sensitive functional groups. Furthermore, the extended reaction times can compromise selectivity, making the process less efficient for certain substrates.

The choice of the NKR as the model reaction arose from an intriguing mechanistic contrast observed in the literature. Conventionally, the NKR relies on thermal activation, where heat facilitates the rearrangement through a well-established reaction pathway. Here, C=S changes into C=O through a four-center 1,3-oxathietane transition state (TS) in a concerted manner, resulting in the anionic nature of the TS.[37] Due to the anionic nature of the benzene ring, EWGs at the ortho position make the reaction more compatible. However, recent studies have explored unconventional routes involving photoinduced charge carrier mechanisms, such as cation-radical pathways.[32-34] This was first reported by Nicewicz and coworkers, where a pyrilium-based photocatalyst induced an NKR reaction at ambient conditions following a radical cation pathway.[32] Later, many reports came about attempting NKR unconventionally through heat and charge carriers.[34,35] Generally, it has been observed that the nature

of ortho-substituents-whether EWG or EDG is attached dictates the activation energy for the reaction. Hence, these two distinct mechanisms exhibit different substrate preferences — reactions driven by thermal activation are often enhanced by electron-withdrawing groups (EWGs). In contrast, charge carrier-mediated pathways favour substrates bearing electron-donating groups (EDGs).

Building on this understanding, we hypothesized that exploring these two activation mechanisms in parallel — one via localized heat generation (by NPs) and the other via charge carrier generation (by QDs) — could unlock new insights into reaction selectivity and efficiency. For this purpose, the nature of the substrate chosen for our interest was an EDG-OMe present at the ortho position, where we expect a QD-driven reaction to be of higher yield relative to thermally driven by NP.

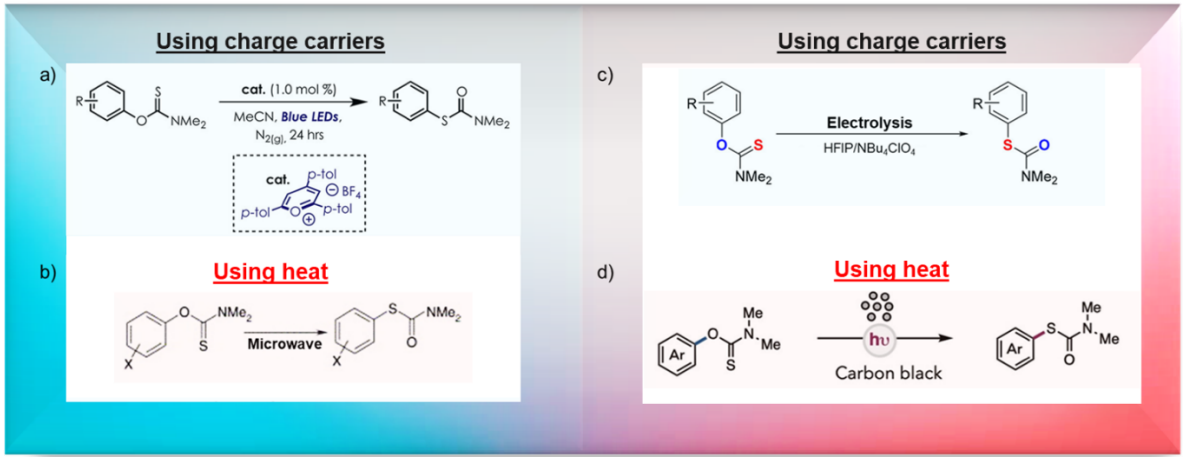

Figure 3: Unconventional approaches to NKR from literature. a) Using charge carriers-photocatalyst. [32] b) Using microwave heat.[36] c) Using electrochemical method.[33] d) Using a photothermal reagent- carbon black.[35]

Chapter 2: Materials and Methods

1) Materials and Reagents

Gold chloride trihydrate ($HAuCl_4.3H_2O$), oleylamine (OAm), indium (III) iodide (InI_3), tris-(dimethylamino) phosphine, acetonitrile (ACN), dimethyl formamide (DMF), dodecane, dry sodium hydride (NaH) and 1,3,5-trimethoxybenzene (TMB) from Sigma-Aldrich; Zinc iodide (ZnI_2), 4-methoxyphenol, dimethylthiocarbamoyl chloride, and dimethylcarbamoyl chloride from TCI Pvt Ltd; 4-methoxythiophenol from Chemscene and diphenyl ether (DPE) from SRL Pvt Ltd, were respectively purchased. All experiments were carried out without further purification of supplied reagents.

2) Experimental Section

a) Synthesis of OAm-capped AuNP:

The oleylamine (OAm) capped AuNPs were synthesized using a modified 'hot-colloidal method' by following a literature procedure.[38] In a typical procedure, gold precursors are rapidly injected into a pre-heated surfactant solution. 5 mL OAm was refluxed at 150 ^{0}C in a 100 mL flask under argon. Then, a mixture of 0.3 mmol of $HAuCl_4.3H_2O$ in 1 mL OAm was rapidly injected into the hot solution, and heating continued for 1.5 hours. A visible color change from yellow to gray and finally to pink was visible, indicating the formation of NPs. (~12 nm size) After cooling the flask to room temperature, 1 mL of hexane was added, and ethanol (~ twice the volume of the reaction mixture) was added to precipitate the particles. The suspension was centrifuged at 5000 rpm for 6 min. The supernatant was discarded, and the nanoparticles were re-dispersed in hexane for further studies. Here OAm acts as a reducing agent as well as a capping agent.

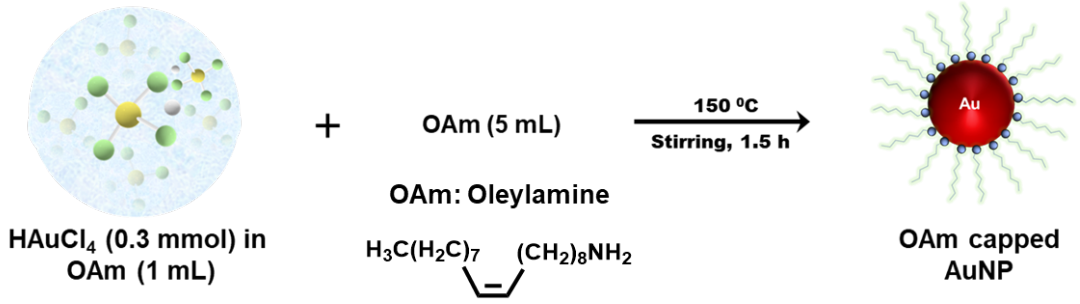

Scheme 1: Synthesis of OAm-capped gold nanoparticles (AuNP).

b) Synthesis of core-only InP QD:

Core-only InP QDs for reaction were synthesized using a modified one-pot synthetic procedure.[41] In a typical procedure, indium (III) iodide (0.45 mmol,169 mg), zinc iodide (2.2 mmol,703 mg), and oleylamine (6.0 mL) were taken in a 100 mL three-neck RB and heated to ~110 ^{0}C under Ar atmosphere with gentle stirring, till a clear solution was formed. The reaction mixture was degassed for ~60 min at 110 ^{0}C, and the temperature was raised further to ~200 ^{0}C under inert conditions. At 200 ^{0}C, tris-(dimethylamino) phosphine (450 µL) in 1 mL of oleylamine was quickly injected into the reaction mixture and kept for ~ 25 minutes. The reaction mixture was then quenched with a water bath, followed by adding 5 mL of hexane to arrest the growth of QD. As synthesized QDs were purified by centrifugation at 7000 rpm for 10 min, followed by precipitation with ethanol to remove unreacted precursors. Finally, the prepared InP QDs were redispersed back in toluene and used for further studies.

c) Synthesis of O-(4-methoxyphenyl) dimethylcarbamothioate (Reactant A) for NKR:

O-(4-methoxyphenyl) dimethylcarbamothioate was synthesized using a modified literature procedure.[26] In a typical synthesis, 4-methoxyphenol (40.3 mmol,5g), dissolved in 20 mL DMF, was taken in a 250 mL round bottom flask and continuously purged with N_2. Followed by, dry NaH (44.33 mmol,1.1 eq.) was added part by part, and the temperature was maintained between 0-4 ^{0}C. The addition of NaH resulted in H_2 gas evolution, and once it was ceased, dimethylthiocarbamoyl chloride (52.4 mmol, 1.3 eq.) was added to the reaction mixture and was kept under stirring for 2-3 h. The progress of the reaction was analyzed using a thin-layer chromatographic (TLC) technique with a 15% hexane/ethyl acetate eluent system.

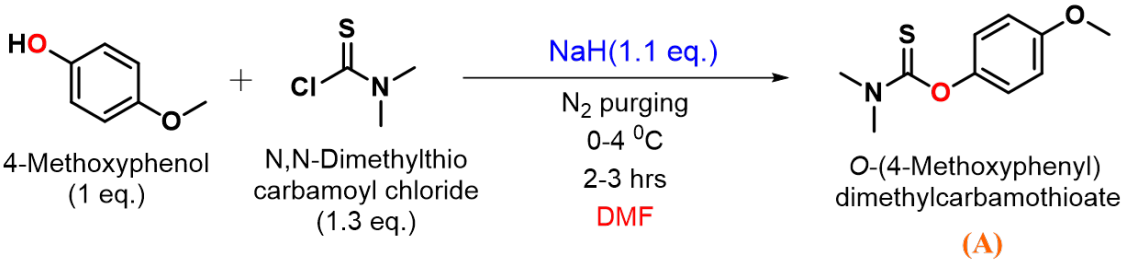

Scheme 2a: Synthesis of O-(4-methoxyphenyl) dimethylcarbamothioate (reactant A).

Ultimately, the reaction was quenched with ice and stored at 4 ^{0}C overnight to allow complete precipitation of the desired product. The precipitate was filtered and dried in a vacuum. This results in the formation of a yellowish-white solid. Finally, the pure product, crystalline white solid, was obtained by column chromatography using 8% hexane/ethyl acetate as the eluent and characterized with ^{1}H-NMR, GC, and HRMS (refer to appendix). Similarly, the desired rearranged product was also synthesized for characterization and quantification.

d) Synthesis of S-(4-methoxyphenyl) dimethylcarbamothioate (Desired Product B):

In a typical synthesis, 4-methoxythiophenol (7.13 mmol,1g), dissolved in 10mL DMF, was taken in a 100 mL round bottom flask and continuously purged with N_2. Followed by, dry NaH (7.84 mmol,188 mg) was added part by part, and the temperature was maintained between 0-4 ^{0}C. The addition of NaH resulted in H_2 gas evolution, and once it was ceased, dimethyl carbamoyl chloride (9.27 mmol, 1.3 eq.) was added to the reaction mixture and was kept under stirring for 2-3 h. The progress of the reaction was analyzed using a thin-layer chromatographic (TLC) technique with a 12% hexane/ethyl acetate eluent system. Ultimately, the reaction was quenched with ice and stored at 4 ^{0}C overnight to allow complete precipitation of the desired product. The precipitate was filtered and dried in vacuum. Finally, the pure product was obtained by column chromatography using 4% hexane/ethyl acetate as the eluent and characterized with ^{1}H-NMR, GC, and HRMS. (refer to appendix)

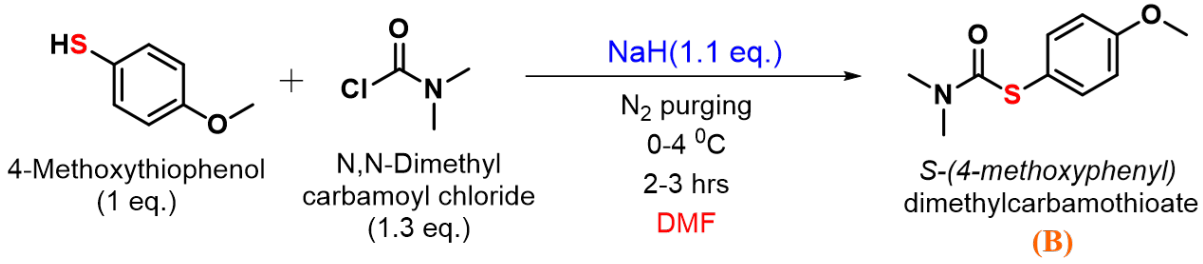

Scheme 2b: Synthesis of S-(4-methoxyphenyl) dimethylcarbamothioate (desired product B).

e) Photocatalytic NKR with core-only InP QDs:

In a 5mL test tube equipped with a stir bar, 20 mg (0.01 mmol) of O-(4-methoxyphenyl) dimethylcarbamothioate was dissolved in 1.5 mL acetonitrile (ACN), to which 11 µM (0.03 mol %) of InP QDs were added. The reaction mixture was irradiated with 2 x 10 W 390 nm LEDs for 12 hours. (400 mW power irradiated)

Preliminary photocatalytic conversion was examined through thin-layer chromatography. The % conversion and desired product yield were calculated from ^{1}H-NMR studies using 1,3,5-trimethoxybenzene as the internal standard. Typically, ACN was evaporated under a vacuum, and the residue of the crude reaction mixture was dissolved in $CDCl_3$ to obtain ^{1}H-NMR spectra. GC-MS analysis was also performed to validate the photocatalytic performance. Control experiments were carried out without QD (with light irradiation) and in the dark (with QD) under similar experimental conditions.

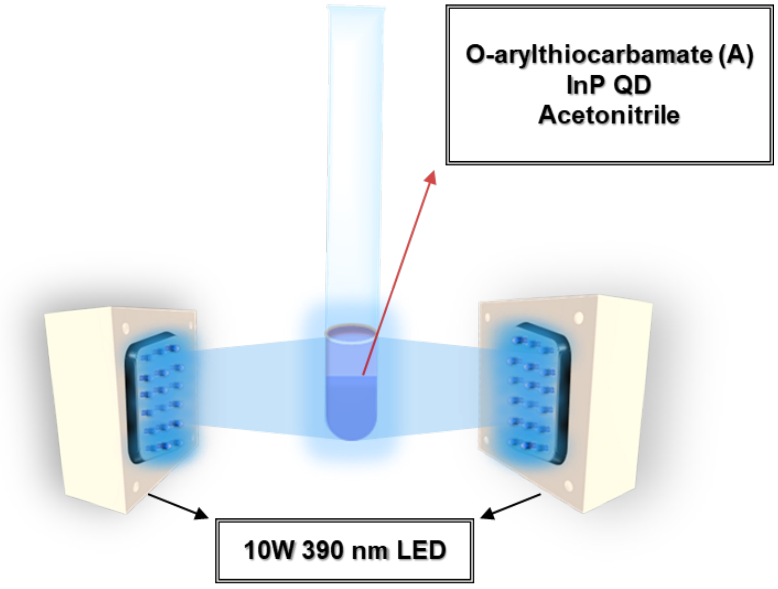

Scheme 3: A general scheme of reaction set up of photocatalytic NKR with reaction mixture in a test tube

f) Photothermal NKR with OAm-capped AuNPs:

In a 15 mL test tube equipped with a stir bar,10 mg (0.05 mmol) of O-(4-methoxyphenyl) dimethylcarbamothioate was dissolved in 1 mL diphenyl ether (DPE), to which x (x is decided by normalization procedure, discussed later) OD of OAm-capped AuNPs were added. The reaction mixture was irradiated for 4 hours with the solar simulator (CEL-PF300-T6) at AM=1.5 by focussing through two parallel lenses (radius is 2.5 cm), which are kept in line with the test tube setup (**Figure 4a, b**). The light was focussed at a distance of ~ 9 cm (measured from the lens), with the beam diameter measured to be ~1.2 cm, and the optical power illuminated was noted to be ~7 $W.cm^{-2}$. A thermopile optical power detector (Model LM-10 HTD; Coherent, Santa Clara, CA 95054 USA) was used to measure the power of light falling on the test tube after focusing. (**Figure 4c**)

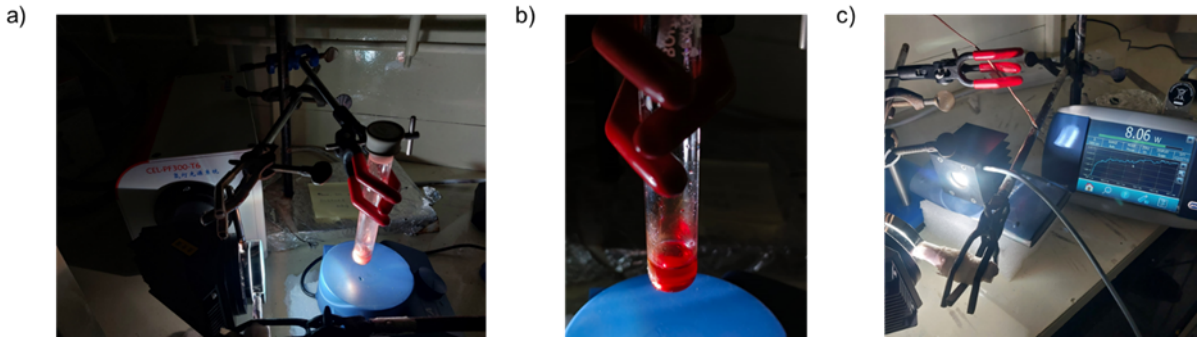

Figure 4: Reaction setup of photothermal NKR. a) Side view of the setup with the solar simulator(left), lenses to focus(middle), and test tube with the reaction mixture(right). b) Reaction mixture (Reactant A+ diphenyl ether + AuNP) before irradiation. c) Power of irradiation measured using a thermopile optical power detector.

The reddish color (due to plasmonic NPs) in the reaction mixture changes to brownish yellow at the end of the reaction. The reaction mixture was then first centrifuged at 10000 rpm for 4-5 minutes to settle the NPs; the remaining supernatant was purified by column chromatography (silica column, 4% ethyl acetate in hexane), and the product was characterized by using ^{1}H-NMR (**Figure 7**) and HRMS techniques. (refer to appendix) Control experiments were carried out without NPs (with irradiation) and in the dark (with NPs) under similar experimental conditions. The thermal experiment with a typical electrical heater was also performed in the laboratory at 210 ^{0}C.

g) Gas Chromatography-Mass Spectrometry (GC-MS) Measurements:

The reaction mixture (A, B, NP, and DPE) is first centrifuged at 10000-12000 rpm for a few minutes, and the NPs are separated. The remaining supernatant is half-diluted with acetonitrile and added with ~10.53 mM of dodecane (IS), out of which one µM is injected via a needle into the Shimadzu GCMS-2010 plus for analysis.

3) Characterization techniques

a) Transmission electron microscopic (TEM) studies:

The AuNPs were characterized using high-resolution transmission electron microscopy (HR-TEM) microscopy studies on the JEOL JEM-2200FS (200 kV) HRTEM instrument. AuNPs were drop cast on a 400-mesh carbon-coated copper grid (Ted Pell Inc.) and dried under vacuum overnight to prepare the TEM sample.

b) UV-visible absorption spectroscopy:

All UV-visible absorption spectra were recorded using SHIMADZU UV-3600 plus UV-VIS-NIR spectrophotometer over the range 200-800 nm. The AuNPs for measurements were taken in a 3 mL quartz cuvette with a path length of 1 cm.

c) X-ray diffraction (XRD) measurements:

X-ray diffraction patterns were measured on Bruker D8 Advanced X-Ray Diffractometer using Cu Kα (λ = 1.54 Å) rays. The samples for XRD analysis were prepared by drop-casting the as-synthesized QDs on a clean glass substrate.

d) Fourier-transform infrared spectroscopy (FTIR) studies:

Fourier transform infrared spectroscopy (FTIR) experiments were performed to confirm the presence of ligands on the surface of QDs. The measurements were performed on the NICOLET 6700 FTIR instrument using a solid KBr disc.

e) Nuclear Magnetic Resonance Spectroscopy (NMR) studies:

NMR spectra for the reaction mixture and purified products were recorded on 400 MHz JEOL ECS-400, Bruker 400 MHz instruments.

f) Gas Chromatography-Mass Spectrometry (GC-MS) Measurements:

The GCMS data was recorded using Shimadzu GCMS-2010 plus using He as a carrier gas.

g) High-Resolution Mass Spectrometry (HRMS):

The HRMS experiments were performed using an ESI-TOF mass analyzer.

h) Cyclic Voltammetry Measurements:

The CV measurements were performed using Metrohm DropSens μStat400 electrochemical workstation and Dropview 8400 software of version 2.215B1204. Glassy carbon was used as the working electrode, Ag/AgNO3 as the reference electrode, and Pt wire as the counter electrode.

4) Calculations for reaction yield and NP concentration

1) Procedure for reaction yield calculation

The reaction yield was calculated using proton NMR spectroscopy and gas chromatography techniques. Since we are interested in the crude yield of the major product, the reaction mixture (RM) was not subjected to any purification (for yield calculation).

a) By Gas Chromatography (GC)

For calculating the reaction yield from GC, a known amount of an internal standard (IS), dodecane, was added to the RM to find the concentration of product formed ($\mathbf{C_{product}}$). Having separately synthesized the reactant (A) and the desired product (B), calibrating A and B gives the relative response factor (***RRF***). The ***RRF*** is a correction factor introduced to account for the differences in detector sensitivity for different molecules (analyte, impurities, or IS), thus allowing an accurate quantification. The GC data gives information about the area of the product peak and the area of the IS peak, substituting all these values in the equations (**Figure 5a**) to give the product yield (%).

$$\textbf{Concentration of product formed } (\mathbf{C_{product}}) = \textit{Peak area of product} \times \frac{\textit{Conc. of IS}}{\textit{Peak area of IS}} \times \frac{1}{RRF}$$

$$\textbf{Relative Response factor } (RRF) = \frac{\textit{Peak area of product} / \textit{Conc.of product}}{\textit{Peak area of IS} / \textit{Conc of IS}}$$

$$\textbf{Product Yield (\%)} = \frac{\mathbf{C_{product}}}{\mathbf{C_{reactant}}} \times 100$$

Figure 5a: Formulas for reaction yield calculation using Gas chromatography (GC).

b) By ^{1}H-NMR Spectroscopy

For calculating the reaction yield from ^{1}H-NMR, a known amount of an IS, 1,3,5-trimethoxybenzene (TMB: used for QD) or 1,1,2,2-tetrachloroethane (TCE: used for NP) was added to the RM in $CDCl_3$. The signals to find the internal standard TCE and TMB are δ 5.93 (2H, singlet) and δ 6.07 (3H, singlet) ppm, respectively. These peaks are distinct and don't overlap with the NMR peaks of any other compound in the

reaction mixture. For a more precise understanding, a ^{1}H NMR spectrum for one of the cases is given along with calculations. (refer to appendix)

The reaction under consideration is a 1:1 reaction, which implies that for every mole of reactant consumed, an equivalent mole of product is formed. We know the number of moles of reactant taken and the moles of IS added, but the number of ***Moles* of product** has to be determined from the NMR spectrum. Any such reaction's yield (%) is calculated as in the equations. (**Figure 5b**)

$$\textit{Moles}\ \text{of product} = \textit{Moles}\ \text{of}\ \textit{IS added}\ \text{x}\ \frac{\textit{Integral value of product}\ /\ \textit{Number of protons of product}}{\textit{Integral value of IS}\ /\ \textit{Number of protons of IS}}$$

$$\text{Product Yield (\%)} = \frac{\textit{Moles}\ \text{of product}}{\textit{Moles}\ \text{of reactant taken}}\ \text{x}\ 100$$

Figure 5b: Formulas for reaction yield calculation using ^{1}H NMR.

2) <u>Normalization procedure for AuNP concentration studies</u>

Since the concentration of NP used for each set of experiments has to be the same, we have used a normalization procedure to keep the amount of NP used constant. This is done as follows:

The concentration of AuNPs in stock solution was calculated using Beer-Lambert's law:

$$\boldsymbol{A = \varepsilon . c . l}$$

where,

A is the absorbance

ε is the molar extinction coefficient ($M^{-1}cm^{-1}$)

c is the concentration of the solution (M)

l is the optical path length (cm).

The molar extinction coefficient (***ε***) for AuNP was taken to be 2.7×10^8 $M^{-1}cm^{-1}$ for ~12 nm diameter particles. The concentration of AuNP stock solution was estimated (in terms of AuNPs) to be ~0.58 μM. From the absorbance spectrum, we get to how much AuNP concentration has to be added to the reaction mixture to make it 1 OD, which is ~ 3.7 picomoles.

For the optimized amount of AuNP in the reaction mixture (RM), the condition was found to be 12 OD, which corresponds to ~44 picomoles.

In short, to avoid manual error while taking AuNP, the absorption spectrum is taken prior for all sets of experiments, and the amount of AuNP for 12 OD added to RM is fixed after calculating from Beer-Lambert's Law.

Chapter 3: Results and Discussions

I. Approach 1: Using heat

To investigate whether heat, specifically thermoplasmonic heat, can drive the Newman-Kwart rearrangement (NKR) reaction, plasmonic AuNPs were chosen as the heat-generating material. AuNPs were synthesized, characterized, and further used for thermoplasmonic studies.

1) Synthesis and characterization of AuNP

AuNPs (~ 11-12 nm in diameter) were synthesized using a 'hot-colloidal method.[38] The nanoparticles were surface-functionalized with oleylamine (OAm) to enhance their colloidal stability in an organic medium, ensuring compatibility with non-aqueous reaction conditions. The surface plasmon resonance (SPR) band of the synthesized AuNPs was observed at ~ 527 nm (**Figure 6a**), indicating strong absorption in the visible region. This plasmonic feature aligns well with the solar spectrum, suggesting the possibility of using sunlight as an irradiation source in future experiments. (unlike what's done in this study) Transmission electron microscopy (TEM) images confirmed the formation of uniform, homogenous, and spherical AuNPs with an average diameter of 11.2 $\pm$ 0.4 nm. (**Figure 6b, c**) The SPR peak (~527 nm) and the TEM size distribution closely match the values for AuNPs synthesized as in the literature report.[38]

With the synthesis and characterization of AuNPs established, their role in driving the NKR reaction via thermoplasmonic heat was investigated.

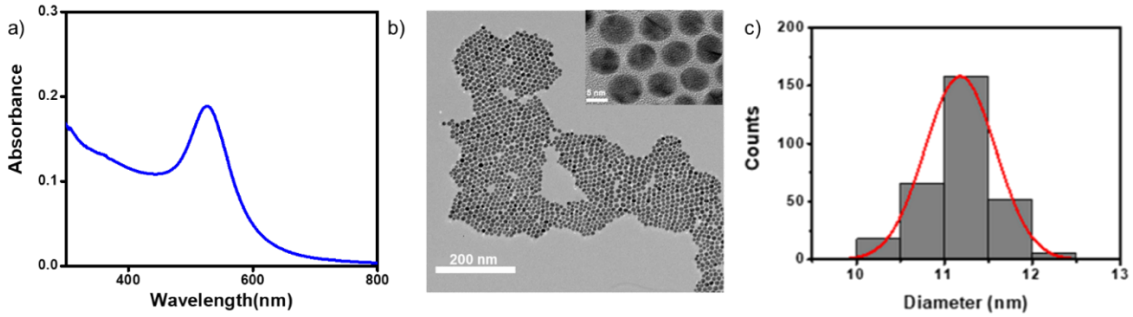

Figure 6: Characterization of synthesized AuNPs. a) UV-visible absorption spectra of AuNPs. b) TEM images showing NPs of size ~ 12 nm. c) Histogram for size distribution of NPs. (calculated from ~300 particles)

2) NKR driven by thermoplasmonic heat

Optimization studies were conducted to determine the ideal reaction conditions and investigate whether thermoplasmonic heating from AuNPs can drive the Newman-Kwart rearrangement (NKR) reaction. Initially, reactions were performed under stirred and unstirred conditions at 8 OD concentrations for 6 hours. It was observed that stirring significantly improved the reaction yield (refer to appendix), suggesting that better heat and mass transfer enhanced reaction efficiency. Based on these observations, stirring was included in all subsequent reactions. Concentration-dependent and kinetics studies, as well as control experiments, followed this. (discussed in the subsequent section) The final optimized conditions consisted of 12 OD AuNP concentration, 4 h of irradiation under a solar simulator (~7 W/cm²), and continuous stirring of reactant O-(4-methoxyphenyl) dimethylcarbamothioate dissolved in diphenyl ether (DPE) as the solvent. (**Scheme 4**)

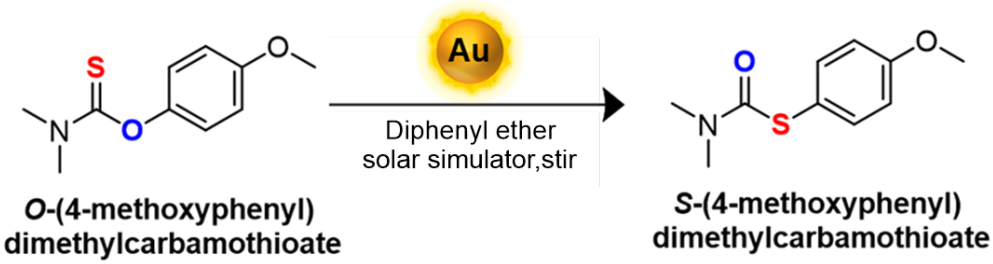

Scheme 4: Reaction Scheme for photothermal NKR using the solar simulator as the irradiation source.

The reaction progress was visually indicated by a color change from red (AuNP plasmonic absorption) to brownish-yellow. A similar color change was seen during the control experiment (Without AuNP + heat; conventional thermal conditions) from colorless (reactant dissolved in DPE) to brownish-yellow, suggesting that the change was primarily due to the reaction rather than nanoparticle degradation. However, upon prolonged heating, AuNPs were observed to settle at the bottom of the reaction vessel, indicating potential aggregation, though further experimental confirmation is needed to establish this effect definitively.

The reaction yield was determined using GC and ^{1}H-NMR spectroscopy, both of which showed consistent results (23% GC yield vs. 22% NMR yield), confirming the reliability of the quantification. Hence, for ease of performing and convenience, we have calculated yield % from GC measurements in the remaining studies. (refer to

appendix) After purification, ^{1}H NMR of the reaction mixture matches the desired product. (**Figure 7**) Temperature monitoring using a thermocouple immersed in the reaction mixture revealed that the reaction took approximately 30-45 minutes to reach ~210^{0}C (**Figure 9b**), which aligns with the operating temperatures typically used for thermally activated NKR reactions.[36] The formation of solvent vapors at this stage suggests that localized regions within the reaction mixture may have exceeded the bulk-measured temperature, potentially approaching the boiling point of DPE (~250^{0}C). Since thermocouples measure bulk temperatures rather than nanoscale heating effects, it is possible that plasmonic heating near the AuNPs resulted in localized temperature spikes above the measured value, leading to enhanced reaction activation.

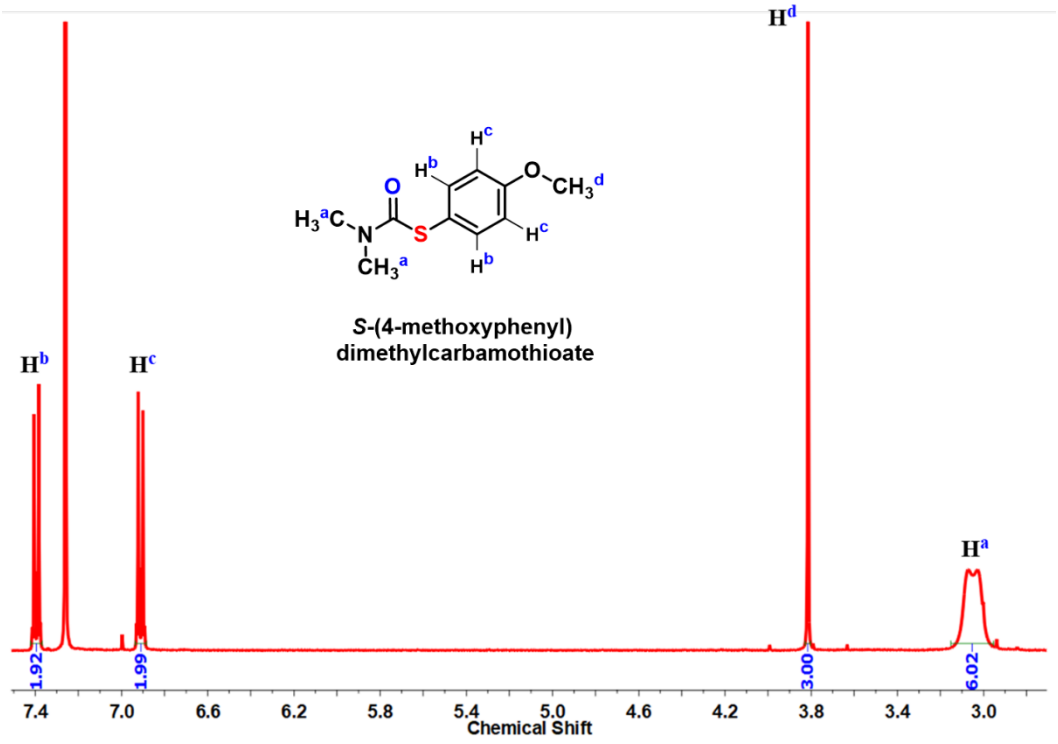

Figure 7: Purified ^{1}H NMR of product.

3) <u>Concentration-dependent and kinetics studies</u>

To determine the impact of plasmonic nanoparticle concentration on reaction efficiency, the NKR reaction was performed using AuNPs at different optical densities (ODs): 4, 8, 12, and 16 OD for a time of irradiation of 4h. The yield was having a trend, increasing from 4% (4 OD) → 13% (8 OD) → 20% (12 OD) before declining to 11% (16 OD). This suggests that while an increase in AuNP concentration enhances

plasmonic heat generation and reaction rate, excessive concentrations may lead to overheating, increasing decomposition, and reduced product selectivity. Thus, 12 OD was determined to be the optimal concentration for the reaction. (**Figure 8a**)

A time-dependent kinetic study was conducted at 12 OD for 1 to 6 h. (**Figure 8b**) The reaction yield followed an increasing trend up to 4 hours (6.8% → 14.2% → 17.3% → 23%), beyond which a sharp decline in yield was observed (13.4% at 5h, 14.5% at 6h). This drop in yield correlated with a significant increase in decomposition, which rose from 16.7% at 4h to 39.3% at 6h, suggesting that prolonged irradiation leads to side reactions and product degradation. These results indicate that 4 hours is the optimal reaction time, balancing conversion efficiency and minimizing decomposition.

After conducting the concentration and kinetic studies, control experiments were performed to definitively establish the role of AuNPs in driving the NKR reaction.

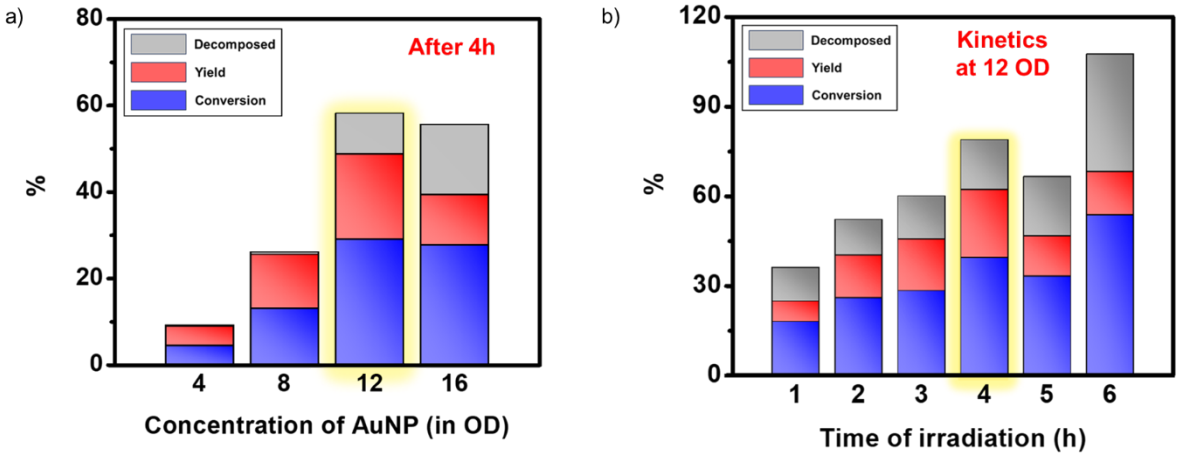

Figure 8: Concentration and time-dependent studies. a) Bar diagram showing % decomposition, yield, and conversion at different AuNP concentrations (4,8,12,16 ODs) in 4h of irradiation. b) Kinetics study done at 12 OD concentration of AuNP up to 6h.

4) Control experiments and conclusions

A series of control experiments were conducted to verify the role of plasmonic heating in driving the NKR reaction. (**Figure 9a**) Under light irradiation without AuNPs, only a ~ 2% yield was observed, indicating that direct photochemical activation of the substrate is minimal. Also, no transformation was seen in the reaction, which was kept in the dark, reaffirming the role of light. Conventional bulk heating at 210^0C (kept at the same temperature as measured in thermocouple) under electrical heating yielded 12.6%, which, while higher than the light-only condition, was still significantly lower

than the plasmonic heating result (23%). This suggests that plasmonic heating enhances the reaction efficiency, likely due to localized nanoscale heating effects, which are absent in conventional thermal setups. Furthermore, the lifetime of 'hot carriers' (in fs scale) is relatively lower while using AuNP as 95 % of the process is a dominant pathway that NKR here behaves as a purely thermally driven reaction[14]; the involvement of hot carrier transfer is unlikely, reinforcing the conclusion that the observed enhancement is due to heat generation from plasmonic AuNPs rather than electronic effects.

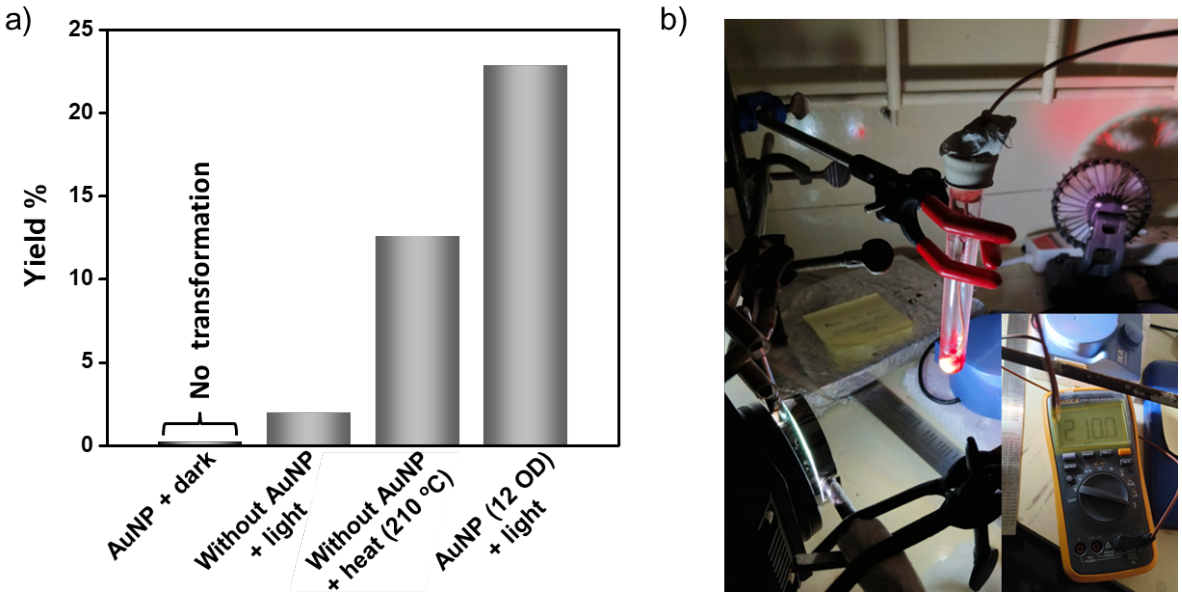

Figure 9: Control experiments and temperature measured. a) Bar diagrams representing the % yield of the rearranged product under different reaction conditions. (control experiments) b) Bulk temperature measured to be 210^0C by a thermocouple.

A comparison with literature-reported NKR reactions provides additional insights into the reaction efficiency. Traditional thermal conditions typically require ~270^0C for 2-3 hours to achieve 72-90% yields.[26,27,36] In contrast, plasmonic heating in this study reached only ~210°C, resulting in a lower yield (23%) and increased decomposition over time. This indicates that plasmonic heating, while effective, may not provide sufficient temperature to drive the reaction at the same rate as bulk heating at 270°C. Additionally, the non-uniform temperature distribution in plasmonic heating (hot spots around AuNPs vs. uniform bulk heating in conventional methods) may contribute to the lower efficiency. Importantly, time-dependent kinetic studies showed that beyond 4 hours, decomposition increased significantly, reinforcing the idea that prolonged

irradiation leads to side reactions and product degradation, which is less of an issue in faster, high-temperature bulk heating.

Although the yield obtained in this study is subpar to traditional oil baths (72-90%) or microwave heating (~75%)[36], it demonstrates the feasibility of light-driven plasmonic heat as an alternative heating strategy. Notably, a recent study by Erin Stache et al. reported ~71% yield within 40 minutes using carbon black as a photothermal reagent [35], outperforming conventional heating and plasmonic AuNP heating. This difference can be attributed to carbon black's broad-spectrum absorption and high thermal conductivity, allowing for rapid and uniform heat generation. In contrast, AuNPs exhibit localized heating effects due to their specific surface plasmon resonance (~527 nm), leading to a different heat distribution mechanism.

Overall, this study highlights the potential of plasmonic heating for thermally driven organic transformations while also underscoring the challenges associated with temperature limitations and prolonged irradiation-induced decomposition. Future work could focus on enhancing heat management, optimizing nanoparticle composition, or integrating hybrid photothermal catalysts to improve reaction efficiency. Despite the moderate yields obtained here, the study establishes plasmonic heating as a promising alternative to conventional bulk heating methods, offering a light-driven, potentially more sustainable route for the high-temperature organic transformation.

II. Approach 2: Using charge carriers

To investigate whether charge carriers generated from quantum dots (QDs) can drive the NKR reaction, InP QDs were chosen as the photocatalyst. Among various photocatalysts reported, our choice of material is QDs as it satisfies most of the fundamental parameters required for an ideal photocatalyst, such as excellent visible light absorption, long-lived charge-separated state, and modular surface chemistry to enhance charge extraction processes. Apart from this, the quantum-confinement effect in QDs provides an excellent way to fine-tune the energy levels for the choice reaction.[10]

InP QDs were specifically chosen for their tunable bandgap, which allows for efficient absorption in the visible region, and their low toxicity, making them a safer alternative to traditional Cd-based QDs.[39,40] Furthermore, their excellent stability in organic

solvents ensured compatibility with non-aqueous reaction conditions. With these properties in mind, InP QDs were synthesized, characterized, and subsequently employed for photocatalytic studies.

1) Synthesis and characterization of core-only InP QDs

InP QDs (~2-3 nm in diameter) were synthesized using a modified one-pot synthetic procedure.[41] The size of QDs was determined to be ~ 2.2 ± 0.2 nm in diameter using powder X-ray diffraction (PXRD) analysis (**Figure 10b**) calculated via the Scherrer equation (refer to appendix). The measured size closely aligns with the reported dimensions of core-only InP QDs in the literature, confirming the successful synthesis of small-sized QDs.[41]

NKR reaction by photocatalysis is believed to proceed through a radical cation intermediate, necessitating the abstraction of a photoexcited hole as the primary step for photocatalytic transformation.[32-34] This means that the oxidation potential of O-arylthiocarbamate must be higher in energy than the valence band of QD. Firstly, we measured the oxidation potential of O-arylthiocarbamate ($\mathbf{E_{ox,1}}$) using cyclic voltammetry (CV), which was found to be -5.54 eV (refer to appendix). As-synthesized InP QDs exhibited the first excitonic peak at 372 nm with an optical band gap of 2.90 eV (calculated from the Tauc plot; **Figure 10a**). The band positions of as-synthesized InP QDs were adapted from a prior literature report from our group, wherein the valence and conduction band positions were estimated to be -6.2 and -3.3 eV w.r.t vacuum, respectively. The energy levels clearly show that the valence band of InP QDs is lower in energy compared to the oxidation potential of O-(4-methoxyphenyl) dimethylcarbamothioate (reactant) and can transfer holes to the reactant upon photoexcitation. Thus, the synthesized InP QDs satisfy the thermodynamic criteria to drive photocatalytic NKR reactions (**Figure 10c**). PXRD analysis further confirmed the crystalline structure of the synthesized QDs, with the obtained diffraction peaks matching well with reference patterns for InP QDs, reinforcing the accuracy of the size determination. (**Figure 10b**) Despite a weak photoluminescence (PL) emission, the absorption profile and calculated band positions confirmed the suitability of these QDs as photocatalysts for driving the NKR reaction.

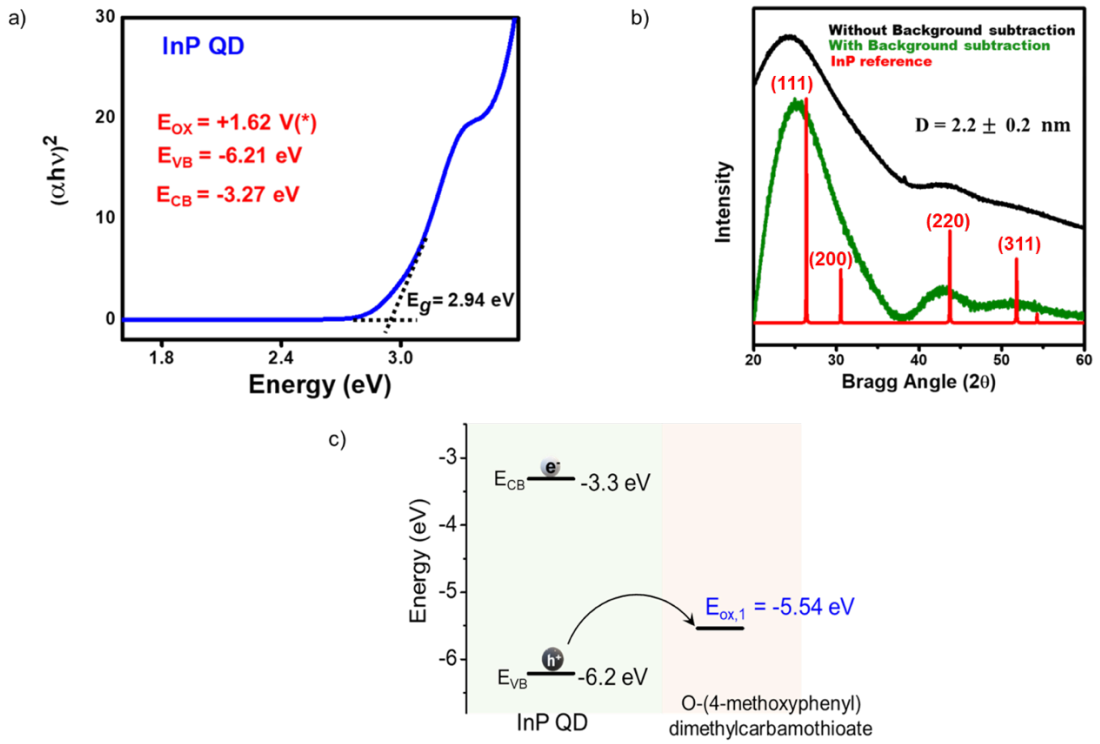

Figure 10: Characterization of synthesized InP QDs and calculation of band positions. a) Tauc plot of the InP QDs (E_{OX} marked as * was taken from the literature report; E_{VB} and E_{CB} were calculated from the plot). b) Powder X-ray diffraction (PXRD) of synthesized InP QDs. c) Band positions of as-synthesized InP QDs compared with oxidation potential of reagent

With their synthesis and characterization established, the QDs were subsequently employed to investigate their role in promoting the NKR reaction via photocatalytic activation.

2) NKR enabled by photocatalysis

After successfully designing and synthesizing InP QDs, we performed the photocatalytic NKR under continuous light irradiation. (**Scheme 5**) A series of optimization studies were initially conducted before coming up with the best condition. These reactions were analyzed preliminarily by TLC and quantitatively using ^{1}H-NMR or GC-MS. The appearance of characteristic signals at δ 7.39 ppm and 3.04 ppm confirms the formation of the rearranged product. (**Figure 13a**)

Initially, different solvents were evaluated, including dichloromethane (DCM), chloroform ($CHCl_3$), and acetonitrile (ACN). Product formation was only observed when ACN was used as the solvent. Both purged (with Ar) and unpurged (air-exposed) conditions were tested across all solvents; however, product formation occurred

exclusively in unpurged ACN, suggesting the involvement of atmospheric oxygen in the reaction. Then, various light sources were explored to determine the optimal irradiation conditions. 2 x 10 W LEDs emitting at 405 nm and 450 nm failed to initiate the reaction. In contrast, irradiation at 390 nm successfully showed product formation. This result aligns with the QD absorption onset (~372 nm), where 390 nm irradiation effectively overlaps with the QD's absorption profile, ensuring efficient light absorption and charge carrier generation. In the unpurged condition, the test tube was covered with aluminum foil and small perforations were made using a needle to allow controlled air exchange.

Based on these studies, the optimized conditions were established as follows: irradiation with 2 x 10 W 390 nm LEDs,0.1mmol reactant A, 1.5 mL ACN as a solvent, air exposure, and ~ 0.03 mol % InP QDs as the photocatalyst. Under these conditions, we observed a decent yield of 54 %, as estimated from ^{1}H-NMR. (**Figure 13b**)

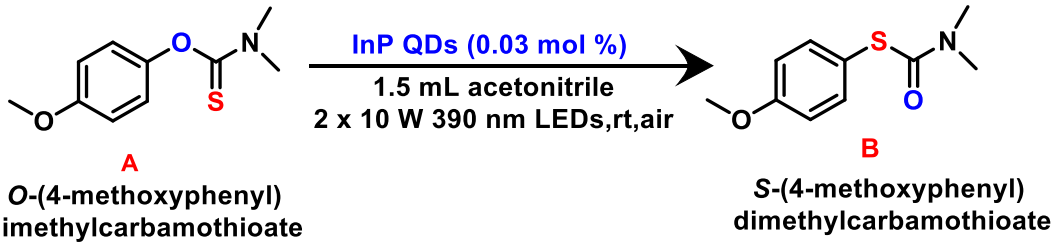

Scheme 5: Reaction Scheme for photocatalytic NKR using InP QDs under optimized conditions.

A series of control experiments were performed wherein negligible conversion/yield was obtained without QD or light. (**Figure 11**) This strongly suggests the active participation of InP QD as a photocatalyst in the NKR reaction.

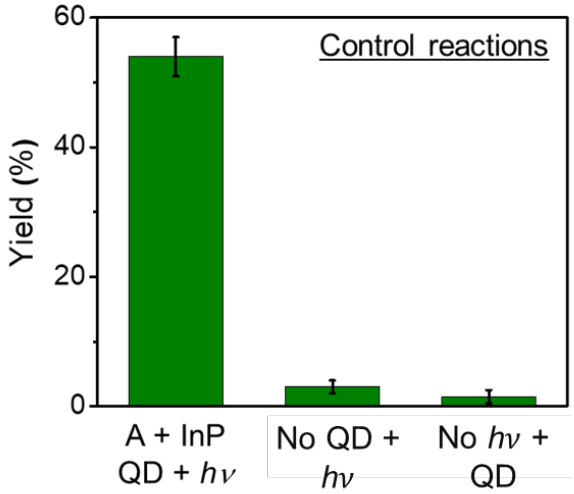

Figure 11: Bar diagrams representing the photocatalytic yield of the rearranged product under different reaction conditions (control experiments).

From the literature reports, we hypothesized that photocatalytic NKR reaction follows a hole-mediated pathway. To validate this point, we synthesized different-sized InP QD possessing valence bands (E_{VB} = -5.52 eV) above the oxidation potential of O-arylthiocarbamate, which makes the transfer of photoexcited holes from InP QD to reactant thermodynamically infeasible. The direct impact of this could be observed from the negligible product yield when different-sized InP QDs were used as the photocatalyst.

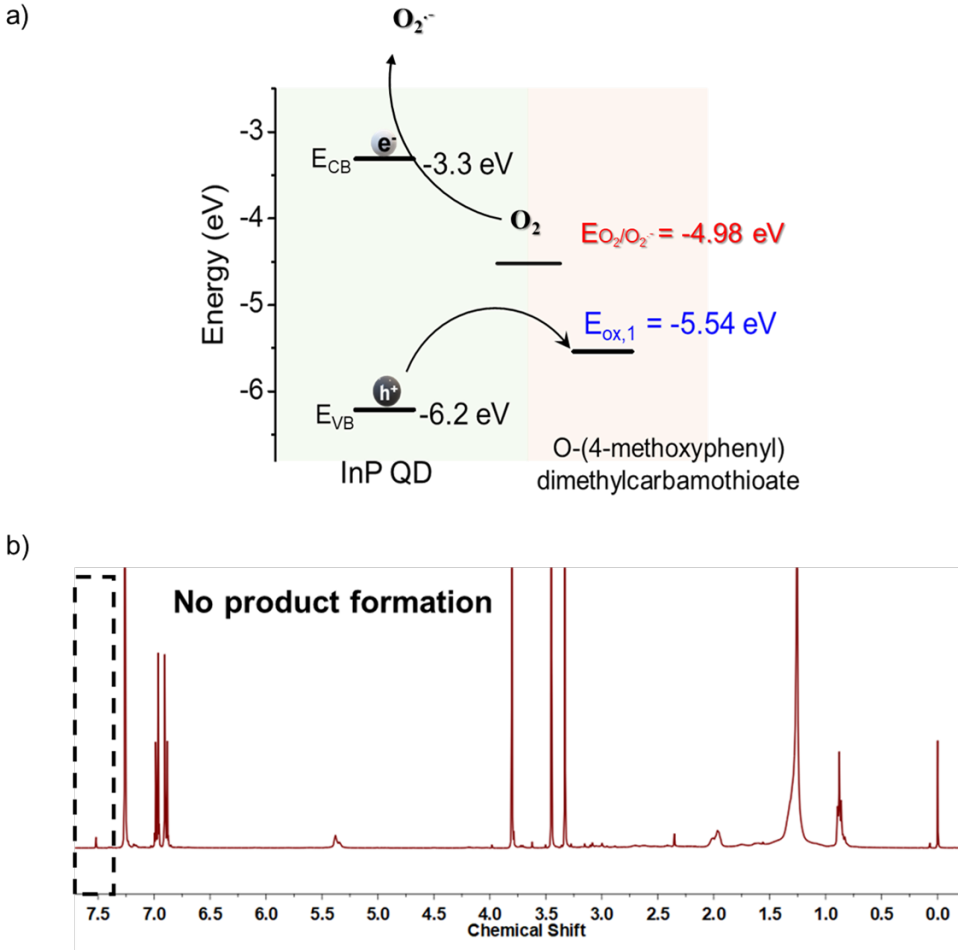

Figure 12: Mechanistic investigation- Role of O_2 in the reaction. a) Representative energy level diagram showing the feasibility of photoexcited hole transfer to reactant molecule and the possibility of O_2 as an electron acceptor in the system. b) ^{1}H shows negligible product formation when purged with Ar gas (absence of O_2).

To elucidate the fate of photoexcited electrons, we purged the reaction mixture with Ar, and interestingly, no photocatalytic activity was observed. (**Figure 12**) This suggests that photoexcited electrons are not involved in the NKR reaction, and O_2 is the probable electron acceptor in our system.

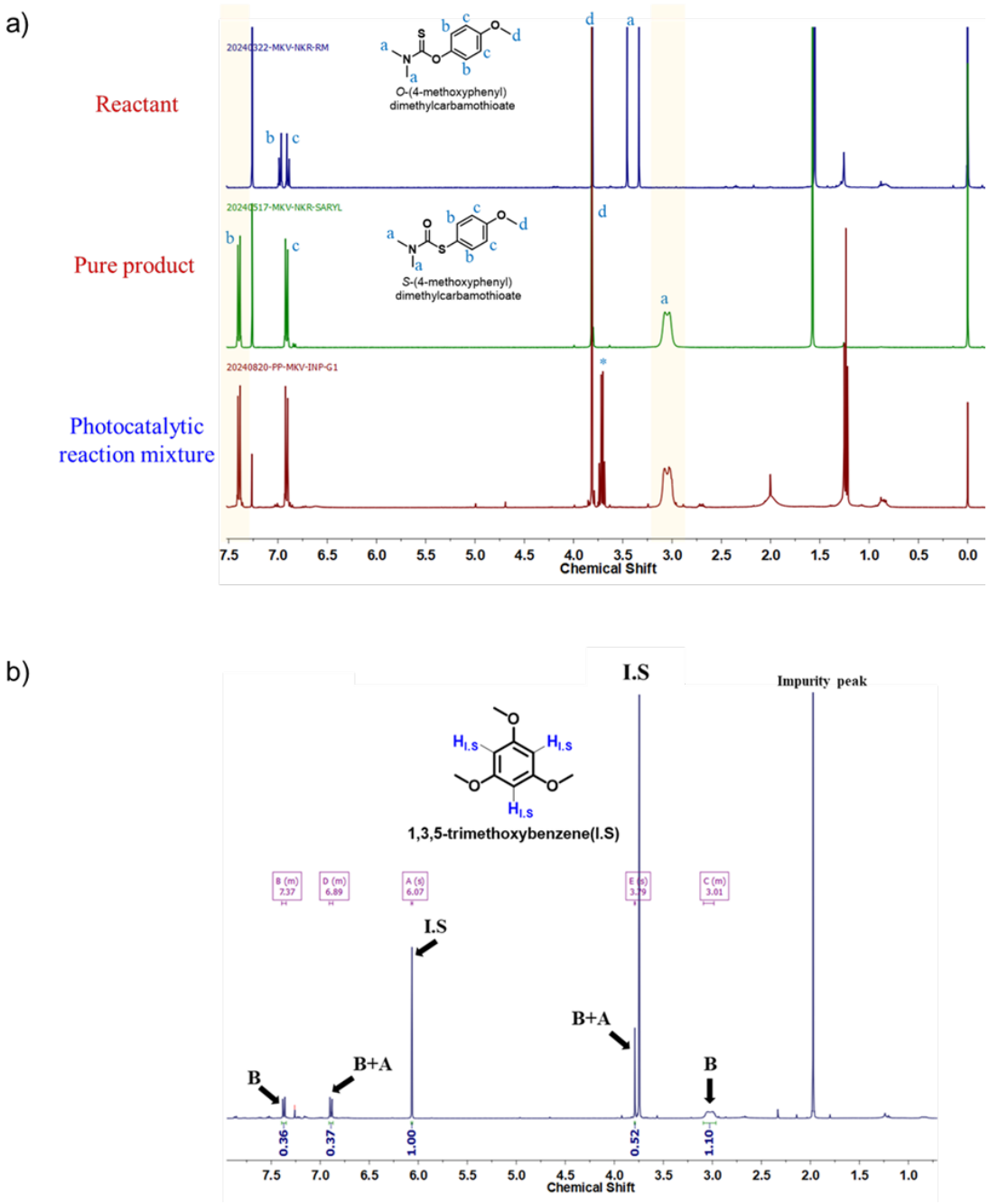

Figure 13: ^{1}H NMR proving product formation and % yield calculated. a) ^{1}H-NMR spectra of the photocatalytic reaction mixture compared to pure reactant and product. b) ^{1}H NMR used for % yield calculation with 1,3,5-trimethoxybenzene as the internal standard (refer to the appendix for calculations). One marked with * is the residual solvent peak

While the yield obtained is moderate compared to conventional thermal methods, this study highlights the potential of InP QDs as photocatalysts for achieving the NKR under milder conditions. Future improvements could focus on enhancing charge carrier dynamics, refining QD surface passivation, or exploring alternative solvents to improve yield and selectivity. While the precise mechanistic details remain under investigation, our findings strongly suggest a hole-mediated pathway with O_2 possibly

acting as an electron acceptor. Further studies are required to confirm the exact sequence of electron transfer steps and identify potential intermediates. Despite these limitations, this work establishes a promising strategy for leveraging light-driven charge carrier generation in this energy-intensive organic transformation.

Chapter 4: Conclusions

This thesis investigated using plasmonic AuNPs and InP QDs as independent systems to drive the Newman-Kwart rearrangement (NKR) through distinct activation pathways — thermoplasmonic heating and photocatalytic charge carrier generation.

In the thermoplasmonic study, AuNPs generated localized heat under light irradiation, achieving a maximum yield of ~23% under optimized conditions (12 OD AuNP concentration, 4 hours of irradiation, and continuous stirring). However, prolonged irradiation led to increased decomposition, indicating that precise control over heat generation is crucial to minimizing side reactions and improving selectivity. Fine-tuning factors such as NP concentration, irradiation conditions, and reactant concentration may help mitigate these issues in future studies.

In the photocatalytic study, InP QDs successfully promoted the NKR reaction, achieving a yield of ~54% under optimized conditions (0.03 mol% QDs, 390 nm LEDs, and ACN as solvent). This improved performance relative to the thermoplasmonic method aligns with literature observations that electron-donating groups (EDGs) such as the –OMe group enhance photocatalytic efficiency. Despite this encouraging result, there is significant potential for further optimization by refining conditions such as reaction time, reactant concentration, and QD surface properties to achieve higher yields and improved selectivity. Mechanistic insights from this study suggest a hole-mediated pathway in the photocatalytic NKR reaction, with O_2 as the likely electron acceptor. However, further experimental validation is required to confirm the precise mechanistic details. This may include additional experiments designed to probe the involvement of reactive oxygen species (e.g., superoxide, singlet oxygen) and confirm the presence of radical intermediates.

Further studies should focus on confirming the distinct reaction pathways for the thermoplasmonic and photocatalytic approaches through mechanistic experiments. Expanding the substrate scope to include EWGs (e.g., $–NO_2$, –CN, –COOH) may enhance thermoplasmonic efficiency, while EDGs could improve photocatalytic performance.

References

1. Nocera, D. G. The Artificial Leaf. *Acc. Chem. Res.* **2012**, *45*, 767–776.

2. Ciamician, G. The Photochemistry of the Future. *Science* **1912**, *36*, 385–394.

3. Devasia, D.; Das, A.; Mohan, V.; Jain, P. K. Control of Chemical Reaction Pathways by Light-Matter Coupling. *Annu. Rev. Phys. Chem.* **2021**, *72*, 423–443.

4. Yang, X.; Wang, D. Photocatalysis: From Fundamental Principles to Materials and Applications. *ACS Appl. Energy Mater.* **2018**, *1*, 6657-6693.

5. Alivisatos, A. P. Perspectives on the Physical Chemistry of Semiconductor Nanocrystals. *J. Phys. Chem.* **1996**, *100*, 13226– 13239.

6. Shim, M.; Wang, C.; Guyot-Sionnest, P. Charge-Tunable Optical Properties in Colloidal Semiconductor Nanocrystals. *J. Phys. Chem. B* **2001**, *105*, 2369– 2373.

7. Bawendi, M. G.; Steigerwald, M. L.; Brus, L. E. The Quantum Mechanics of Larger Semiconductor Clusters ("Quantum Dots"). *Annu. Rev. Phys. Chem.* **1990**, *41*, 477–496.

8. Nirmal, M.; Brus, L. Luminescence Photophysics in Semiconductor Nanocrystals. *Acc. Chem. Res.* **1999**, *32*, 407– 414.

9. Klimov, V. I.; Mikhailovsky, A. A.; Xu, S.; Malko, A.; Hollingsworth, J. A.; Leatherdale, C. A.; Eisler, H. J.; Bawendi, M. G. Optical Gain and Stimulated Emission in Nanocrystal Quantum Dots. *Science* **2000**, *290*, 314– 317.

10. Schaller, R. D.; Klimov, V. I. High Efficiency Carrier Multiplication in PbSe Nanocrystals: Implications for Solar Energy Conversion. *Phys. Rev. Lett.* **2004**, *92*, 186601

11. Baffou, G.; Thermoplasmonics: Heating Metal Nanoparticles Using Light, Cambridge University Press, 2017.

12. Hodak, J. H.; Martini, I.; Hartland, G. V. Spectroscopy and Dynamics of Nanometer-Sized Noble Metal Particles. *J. Phys. Chem. B* **1998**, *102*, 6958–6967.

13. Link, S.; El-Sayed, M. A. Optical Properties and Ultrafast Dynamics of Metallic Nanocrystals. *Annu. Rev. Phys. Chem*. **2003**, *54*, 331–366.

14. Chang, W.-S.; Willingham, B.; Slaughter, L. S.; Dominguez-Medina, S.; Swanglap, P.; Link, S. Radiative and Nonradiative Properties of Single Plasmonic Nanoparticles and Their Assemblies. *Acc. Chem. Res*. **2012**, *45*, 1936–1945.

15. Govorov, A. O.; Richardson, H. H. Generating Heat with Metal Nanoparticles. *Nano Today,* **2007**, *2*, 30–38.

16. El-Sayed, M. A. Some Interesting Properties of Metals Confined in Time and Nanometer Space of Different Shapes. *Acc.Chem.Res*. **2001,***34,*257-264

17. Baffou, G.; Quidant, R. Thermo-Plasmonics: Using Metallic Nanostructures as Nano-Sources of Heat. *Laser Photonics Rev*. **2013**, *7*, 171–187.

18. Yuan, Y.; Jin, N.; Saghy, P.; Dube, L.; Zhu, H.; Chen, O. Quantum Dot Photocatalysts for Organic Transformations. *J. Phys. Chem. Lett*. **2021**, *12*, 7180–7193.

19. Wakerley, D. W.; Kuehnel, M. F.; Orchard, K. L.; Ly, K. H.; Rosser, T. E.; Reisner, E. Solar-Driven Reforming of Lignocellulose to H_2 with a CdS/CdOx Photocatalyst. *Nat Energy* **2017**, *2*, 17021.

20. Bhattacharyya, B.; Simlandy, A. K.; Chakraborty, A.; Rajasekar, G. P.; Aetukuri, N. B.; Mukherjee, S.; Pandey, A. Efficient Photosynthesis of Organics from Aqueous Bicarbonate Ions by Quantum Dots Using Visible Light. *ACS Energy Lett.* **2018**, *3*, 1508– 1514

21. Chakraborty, I. N.; Roy, S.; Devatha, G.; Rao, A.; Pillai, P. P. InP/ZnS Quantum Dots as Efficient Visible-Light Photocatalysts for Redox and Carbon-Carbon Coupling Reactions. *Chem. Mater.* **2019**, *31*, 2258–2262.

22. Jain, V.; Kashyap, R. K.; Pillai, P. P. Plasmonic Photocatalysis: Activating Chemical Bonds through Light and Plasmon. *Adv. Opt. Mater.* **2022**, *10*,2200463.

23. Mukherjee, S.; Libisch, F.; Large, N.; Neumann, O.; Brown, L. V.; Cheng, J.; Lassiter, J. B.; Carter, E. A.; Nordlander, P.; Halas, N. J. Hot Electrons Do the Impossible: Plasmon-Induced Dissociation of H_2 on Au. *Nano Lett*. **2013**,*13*, 240–247

24. Gelle, A.; Jin, T.; De La Garza, L.; Price, G. D.; Besteiro, L. V.; Moores, A. Applications of Plasmon-Enhanced Nanocatalysis to Organic Transformations. *Chem. Rev.* **2020**, *120*, 986–1041

25. Linic, S.; Aslam, U.; Boerigter, C.; Morabito, M. Photochemical Transformations on Plasmonic Metal Nanoparticles. *Nat. Mater*. **2015**, *14*, 567–576.

26. Newman, M. S.; Karnes, H. A. The Conversion of Phenols to Thiophenols via Dialkylthiocarbamates. *J. Org. Chem.* **1966**, *31*, 3980–3984.

27. Kwart, H.; Evans, E. R. The Vapor Phase Rearrangement of Thioncarbonates and Thioncarbamates. *J. Org. Chem*. **1966**, *31*, 410–413.

28. Hori, M.; Ban, M.; Imai, E.; Iwata, N.; Baba, Y.; Fujimura, H.; Nozaki, M.; Niwa, M. *Heterocycles* **1983**, *20*, 2359.

29. Hori, M.; Iwamuru, T.; Imai, E.; Shimizu, H.; Kataoka, T.; Nozaki, M.; Niwa, M.; Fujimura, H. *Chem. Pharm. Bull*. **1989**, *37*, 1245.

30. Sebők, P.; Tímár, T.; Eszenyi, T.; Patonay, T. *Synthesis* **1994**, 837.

31. Newman, M. S.; Hetzel, F. W. Org. Synth. **1971**, *51*, 139.

32. Perkowski, A. J.; Cruz, C. L.; Nicewicz, D. A. Ambient-Temperature Newman–Kwart Rearrangement Mediated by Organic Photoredox Catalysis. *J. Am. Chem. Soc.* **2015**, *137*, 15684–15687.

33. Roesel, A. F.; Ugandi, M.; Huyen, N. T. T.; Májek, M.; Broese, T.; Roemelt, M.; Francke, R. Electrochemically Catalyzed Newman–Kwart Rearrangement: Mechanism, Structure–Reactivity Relationship, and Parallels to Photoredox Catalysis. *J. Org. Chem.* **2020**, *85*, 8029–8044.

34. Enders, P.; Prane, K.; Schönke, E.; Taeufer, T.; Michalik, D.; Rabeah, J.; Francke, R. Cation Radical Newman-Kwart Rearrangement Enabled by Heterogeneous Photocatalysis under Mild Conditions. *ChemCatChem* **2023**, *15*, e202300744.

35. Matter, M. E.; Čamdžić, L.; Stache, E. E. Photothermal Conversion by Carbon Black Facilitates Aryl Migration by Photon-Promoted Temperature Gradients. *Angew Chem Int Ed* **2023**, *62*, e202308648.

36. Moseley, J. D.; Sankey, R. F.; Tang, O. N.; Gilday, J. P. The Newman–Kwart Rearrangement Re-Evaluated by Microwave Synthesis. *Tetrahedron* **2006**, *62*, 4685–4689.

37. Lloyd-Jones, G.; Moseley, J.; Renny, J. Mechanism and Application of the Newman-Kwart O→S Rearrangement of *O* -Aryl Thiocarbamates. *Synthesis* **2008**, *2008*, 661–689.

38. Liu, S.; Chen, G.; Prasad, P. N.; Swihart, M. T. Synthesis of Monodisperse Au, Ag, and Au–Ag Alloy Nanoparticles with Tunable Size and Surface Plasmon Resonance Frequency. *Chem. Mater.* **2011**, *23*, 4098–4101.

39. Thomas, A.; Sandeep, K.; Somasundaran, S. M.; Thomas, K. G. How Trap States Affect Charge Carrier Dynamics of CdSe and InP Quantum Dots: Visualization through Complexation with Viologen. *ACS Energy Lett.* **2018**, *3*, 2368– 2375.

40. Tamang, S.; Lincheneau, C.; Hermans, Y.; Jeong, S.; Reiss, P. Chemistry of InP Nanocrystal Syntheses. *Chem. Mater*. **2016**, *28*, 2491–2506.

41. Roy, P.; Virmani, M.; Pillai, P. P. Blue-Emitting InP Quantum Dots Participate in an Efficient Resonance Energy Transfer Process in Water. *Chem. Sci.* **2023**, *14*, 5167–5176.

Appendix

1) Cyclic Voltammetry (CV) measurements of reactant A

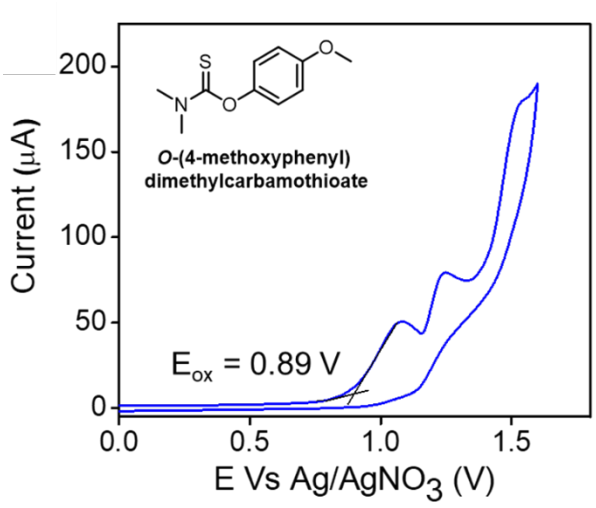

Figure A1: Cyclic voltammogram of the reactant showing the oxidation onset potential of 0.89 V vs $Ag/AgNO_3$.

2) ^{1}H-NMR and GC of reactant (A) and product (B)

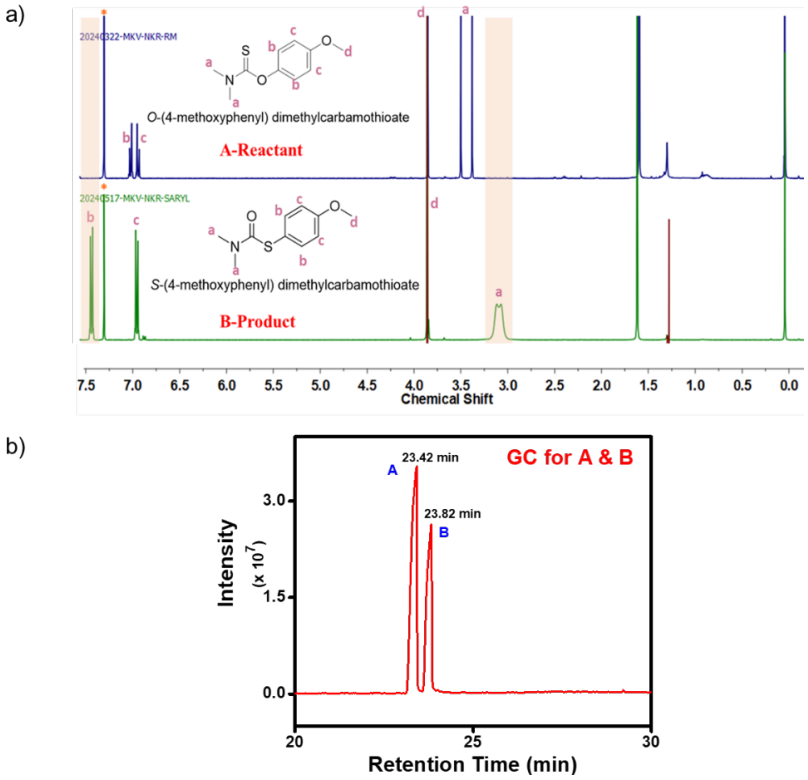

Figure A2: ^{1}H NMR and GC characterization of synthesized A and B. a) ^{1}H NMR of both reactant A and product B separately synthesized are stacked. The highlighted area denotes the distinguishable feature in ^{1}H NMR that confirms product formation. b) Gas chromatography analysis of A and B. The Retention time difference between A and B is seen to be different.

3) HRMS of both reactant (A) and desired product (B) synthesized

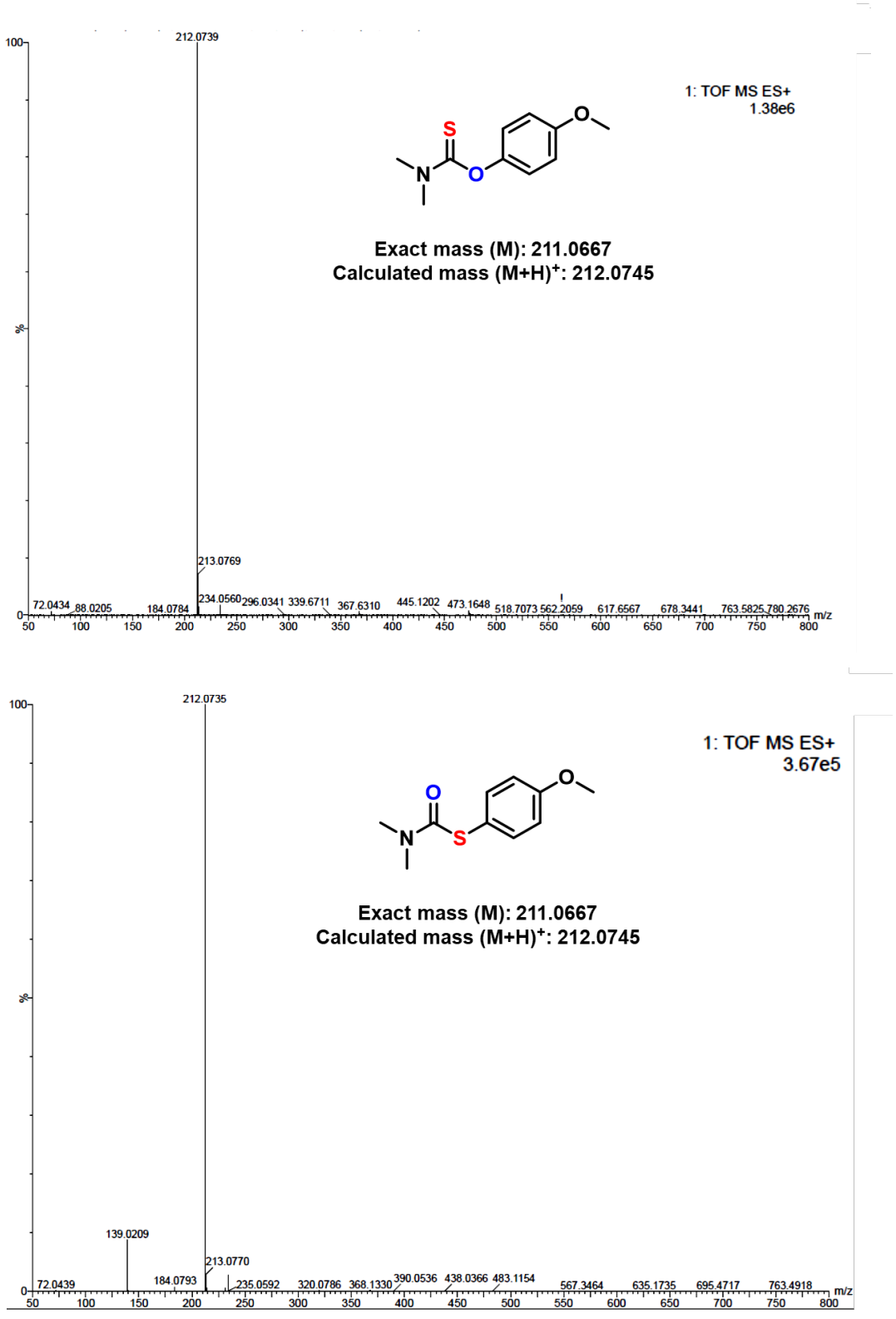

Figure A3: HRMS of synthesized A and B. A(top) and B(bottom). The calculated mass was evaluated as 212.0745 (for both essentially the same as A and B's molecular weights are the same).

4) Approach 1: Using heat

1) Yield % calculated for the optimized condition: by ^{1}H NMR and GC

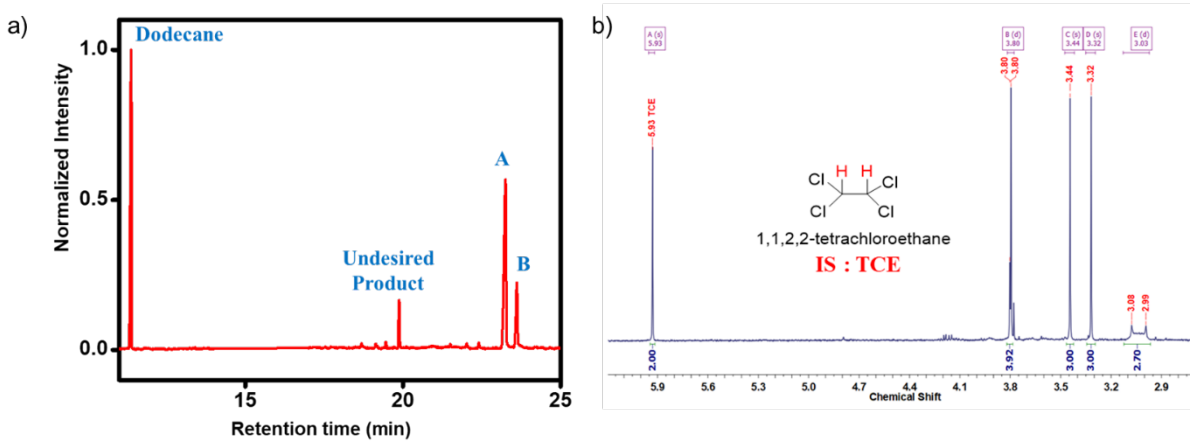

Figure A4: Quantification of % yield in photothermal approach through GC and NMR. a) GC analysis of reaction mixture for the optimized condition. (dodecane is the internal standard, and an undesired side product is seen ~ 19.5-19.6 min, possibly due to decomposition). b)^{1}H NMR of the reaction mixture (TCE is used as the internal standard having 2 protons distinguishable at δ 5.93 ppm, doublet at 3.03 ppm is considered for product peak)

a) By Gas Chromatography (GC)

Here, an internal standard, dodecane, is used to quantitatively measure the yield after injecting the reaction mixture into the GC. After injecting the samples of A and B (synthesized separately) at least 3 times, as per **Figure 5a**, the RRF (relative response factor) for A and B were measured as 0.75 and 0.68, respectively. For the optimized condition for photothermal NKR, the area under the internal standard, product, and reactant peaks were calculated as 0.0422, 0.0455, and 0.0156, respectively. Putting these values in the equation from **Figure 5a,** we get

$$\boldsymbol{Concentration\ of\ B\ formed} = \frac{0.0156\ x\ 10.53}{0.0422\ x\ 0.68} = \mathbf{5.71\ mM}$$

Since half diluted with acetonitrile before injecting, this concentration must be multiplied by 2 to get the actual concentration, which is 11.42 mM.

The concentration of reactant used is 0.05 mmol / 1 mL(volume of DPE taken): 50 mM.

$$\boldsymbol{Yield}\ (\%) = \frac{11.42\ mM}{50\ mM} \times 100 = \mathbf{22.8\ \%\ \sim 23\%}$$

b) By ^{1}H NMR

Here, the number of moles of reactant used is 0.05 mmol, and the number of moles of internal standard: TCE(1,1,2,2-tetrachloroethane) added is 0.47 µmol.
The concentration of reactant used is 0.05 mmol / 1 mL(volume of DPE taken): 50 mM.
Since the peak of internal standard (IS) corresponds to 2 protons and the peak of product at δ 3.03 ppm corresponds to 6 protons, the number of moles of product formed can be calculated using the following equation:

$$\boldsymbol{Number\ of\ moles\ of\ product} = \left(\left(\frac{\boldsymbol{Ip}}{\boldsymbol{6}}\right)\Big/\left(\frac{\boldsymbol{Iis}}{\boldsymbol{2}}\right)\right) \times \boldsymbol{Moles\ of\ IS}$$

Where *I* denote integration value from NMR, subscripts '*p'* denotes the product, and 'is' denotes the internal standard.
Substituting these relevant values from the NMR spectrum, we get:

$$\boldsymbol{Number\ of\ moles\ of\ product} = \left(\left(\frac{2.7}{6}\right)\Big/\left(\frac{2}{2}\right)\right) \times 0.47\ \mu mol = \boldsymbol{0.213\ \mu mol}$$

For this sample, around 20 µL from the reaction mixture was taken, and the remaining 610 µL was the solvent $CDCl_3$, so the dilution factor has to be included, which is 630 (610+20)µL/20µL = 31.5. After considering the dilution factor, the concentration of the product formed will be:

$$\boldsymbol{Concentration\ of\ product\ formed} = \frac{0.213\ \mu mol\ x\ 31.5}{630\ \mu L} = \boldsymbol{10.65\ mM}$$

Dividing this by the concentration of reactant used gives yield; therefore, the percentage yield in this case is:

$$\boldsymbol{Yield}\ (\%) = \frac{10.65\ mM}{50\ mM} \times 100 = \boldsymbol{21.3}\ \% \sim \boldsymbol{21}\%$$

2) HRMS of purified product from the photothermal approach

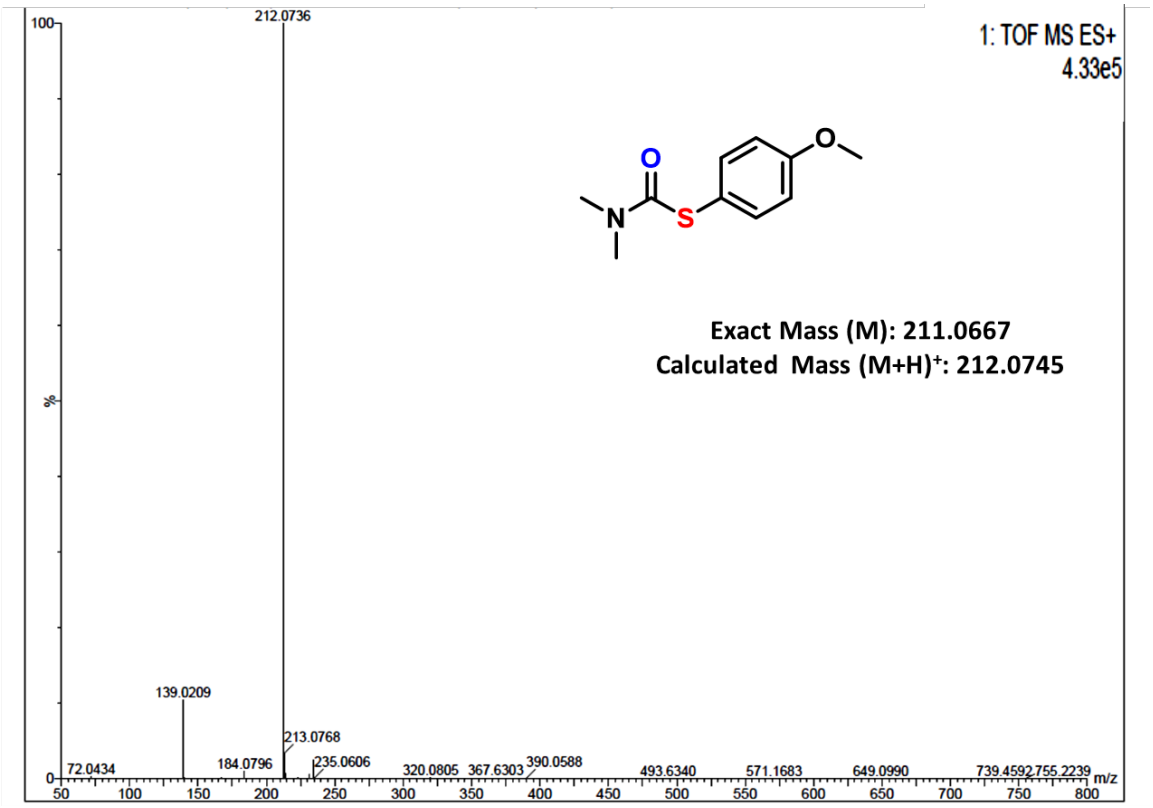

Figure A5: HRMS of purified product. The reaction mixture after column chromatography with 4% ethyl acetate/hexane gives B.

3) Yield % calculated for 6h, 8 OD (stir vs without stir)

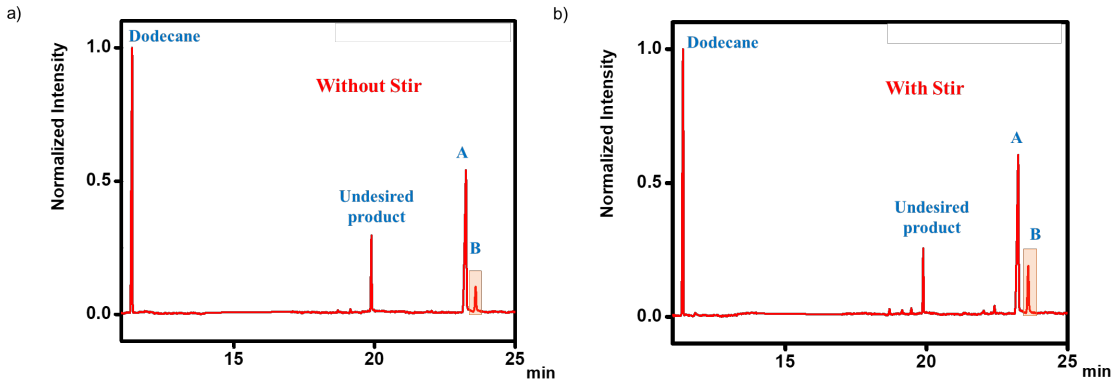

Figure A6: GC quantification of 2 cases, 8 OD concentration of AuNP for 6 h irradiation, with and without stirring of the reaction mixture. a) Without stir. b) With Stir. The highlighted area shows higher product formation for the 'without stirring' case.

Calculations were done similarly to that in section 4.1a) of the appendix and obtained:

Remaining A (mM)	Conversion (%)	Formed B (mM)	Yield (%)	Decomposed (%)
26.36	47.28	6.32	12.64	34.64
Remaining A (mM)	**Conversion (%)**	**Formed B (mM)**	**Yield (%)**	**Decomposed (%)**
31.32	37.36	11.40	22.8	14.56

The table(top) is for without stirring, having ~12%, while the table(below) is for with stirring, having ~22 %.

4) Concentration-dependent and Kinetic studies

All the calculations shown in the table below were from GC using similar methods.

a)

Time: 4 h

AuNP concentration	Conversion (%)	Yield (%)	Decomposed (%)
4 OD	4.6	4.4	0.2
8 OD	13.1	12.5	0.5
12 OD	29.1	19.7	9.4
16 OD	27.8	11.6	16.2

b)

Kinetics (12 OD)

Time of irradiation	Conversion %	Yield %	Decomposed %
1 h	18.1	6.8	11.3
2 h	26.1	14.2	11.9
3 h	28.4	17.3	14.4
4 h	39.5	22.8	16.7
5 h	33.3	13.4	19.9
6 h	53.8	14.5	39.3

Figure A7: GC quantification of concentration-dependent studies and kinetics. a) At 4 h irradiation, yield % is calculated for various concentrations like 4,8,12,16 ODs (the best condition with higher yields and relatively less decomposition is marked in red). b) Kinetics study is done at that optimized AuNP concentration from the previous study; time durations from 1-6 h are taken with 4h seen as the best condition (highlighted in red)

5) Approach 2: Using charge carriers

1) Yield % calculated for optimized condition by 1H NMR

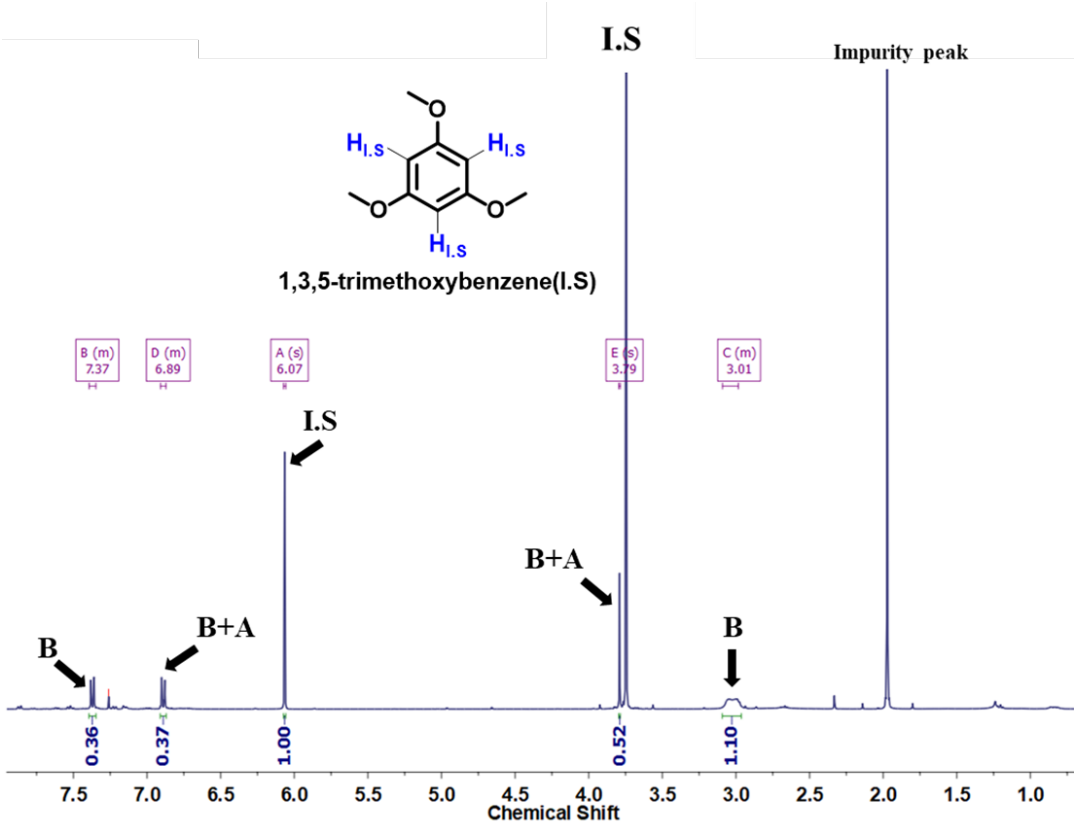

Figure A8: ^{1}H NMR for product formation in the photocatalytic NKR. All peaks, including reactant, internal standard, impurities, and product, are marked.

$$\boldsymbol{Yield}\ (\%) = \frac{\boldsymbol{Number\ of\ moles\ of\ product\ formed}}{\boldsymbol{Number\ of\ moles\ of\ reactant\ used}} \times \mathbf{100}$$

Here, the number of moles of reactant used is 0.1 mmol, and the number of moles of internal standard(1,3,5-trimethoxybenzene) added is 0.1 mmol.

Since the peak of internal standard (IS) corresponds to 3 protons and the peak of product at δ 7.39 ppm corresponds to 2 protons, the number of moles of product formed can be calculated using the following equation:

$$\boldsymbol{Number\ of\ moles\ of\ product} = \left(\left(\frac{\boldsymbol{Ip}}{\mathbf{2}}\right)\Big/\left(\frac{\boldsymbol{Iis}}{\mathbf{3}}\right)\right) \times \boldsymbol{Moles\ of\ IS}$$

Where *I* denote integration value from NMR, subscripts '*p*' denotes the product, and 'is' denotes the internal standard.

Substituting these relevant values from the NMR spectrum, we get:

$$\boldsymbol{Number\ of\ moles\ of\ product} = \left(\left(\frac{0.36}{2}\right)\Big/\left(\frac{1}{3}\right)\right) \times 0.1\ mmol = \mathbf{0.054\ mmol}$$

Dividing this by the number of moles of reactant used gives yield. Therefore, the percentage yield in this case is:

$$\boldsymbol{Yield}\ (\%) = \frac{0.054}{0.1} \times 100 = 54\ \%$$

2) Powder X-ray diffraction (PXRD) analysis

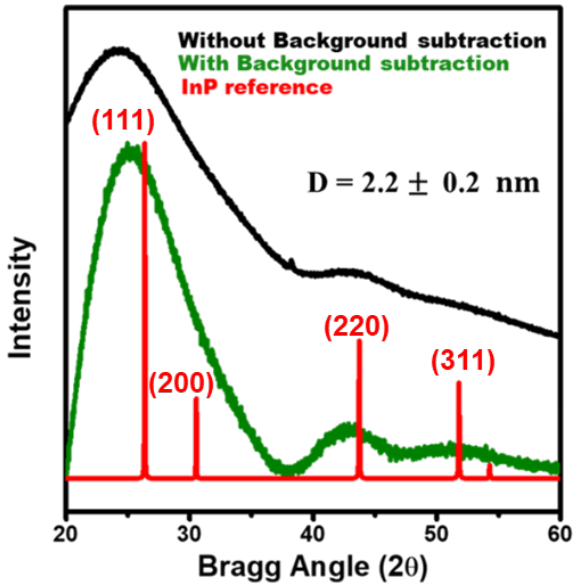

Figure A8: Powder X-ray diffraction (PXRD) patterns of core-InP QDs without (black) and with (green) background subtraction. A comparison of the PXRD patterns of QDs with bulk InP (red) references reveals the presence of a zinc blend phase in InP. The broadness seen in the first peak (at ~ 2θ = 25^0) is due to the combination of signal from (111) and (200) planes of the zinc blend phase and the underlying amorphous glass slide used for sample preparation.

From the figure, the **(220)** plane was considered for calculations.

With L(FWHM) = 3.65^0, so β (in radian) = 0.064 rad

2θ = 44.13^0 (measured from the figure)

PXRD analysis using the Scherrer equation determined the crystalline size of core-only InP QDs.

$$\boldsymbol{D = \frac{k\lambda}{\beta cos\theta}}$$

where D = crystalline size

k = Scherrer's constant (typically considered 0.94 for spherical particles)

λ = Wavelength of Cu k_α X-ray = 1.54 Å

θ = Bragg's angle

β = FWHM of the PXRD peak in radian

Scherrer equation quantitatively gives broadening of a PXRD peak at a particular Bragg's angle, correlating the crystalline size (D) with the width of the peak (β). Substituting all the obtained values in the Scherrer equation, the crystalline size (D) of the core-only InP QDs was calculated as **2.2 ± 0.2 nm.**